JOC The Journal of Organic Chemistry

pubs.acs.org/joc Article

Spiro[1,2]oxaphosphetanes of Nonstabilized and Semistabilized Phosphorus Ylide Derivatives: Synthesis and Kinetic and Computational Study of Their Thermolysis

Jesús García López, Pablo M. Sansores Peraza, María José Iglesias, Laura Roces, Santiago García-Granda, and Fernando López Ortiz*

Cite This: https://dx.doi.org/10.1021/acs.joc.0c01270 Read Online

ABSTRACT: A series of tri- and tetrasubstituted spiro-oxaphosphetanes stabilized by *ortho*-benzamide (*o*BA) and *N*-methyl *ortho*-benzamide (M*o*BA) ligands have been synthesized by the reaction of $C_{\alpha}C_{ortho}$-dilithiated phosphazenes with aldehydes and ketones. They include enantiopure products and the first example of an isolated oxaphosphetane having a phenyl substituent at C3 of the ring. Kinetic studies of their thermal decomposition showed that the process takes place irreversibly through a polar transition state ($\rho = -0.22$) under the influence of electronic, [1,2], [1,3] steric, and solvent effects, with C3/P-[1,2] interactions as the largest contribution to $\Delta G^{\ddagger}$ of olefination. Inversion of the phosphorus configuration through stereomutation has been observed in a number of cases. DFT calculations showed that *o*BA derivatives olefinated through the isolated (N, O)(Ph, C_6H_4, C) oxaphosphetanes (Channel A), whereas M*o*BA compounds decomposed faster via the isomer (C_6H_4, O)(C, N, Ph) formed by P-stereomutation involving a M_{B2} permutational mechanism (Channel B). The energy barrier of P-isomerization is lower than that of olefination. Fragmentation takes place in a concerted asynchronous reaction. The thermal stability of oxaphosphetanes is determined by strong C3/P-[1,2] interactions destabilizing the transition state of olefination. The effect of charge distribution and C3/C4-[1,2] and C4/P-[1,3] steric and solvent interactions on $\Delta G^{\ddagger}$ was also evaluated.

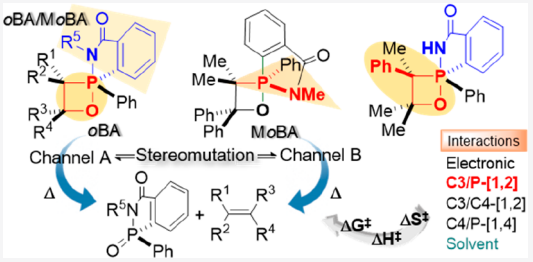

INTRODUCTION

In 1919, Staudinger and Meyer found that the reaction of $Ph_3P{=}CPh_2$ with phenylisocyanate afforded triphenylketenimine and triphenylphosphine oxide and suggested the involvement of a 1,2-oxaphosphetane as an intermediate in the formation of the carbon−carbon double bond (Scheme 1).[1] In a seminal article published in 1953, Wittig and Geissler also proposed the participation of a 1,2-oxaphosphetane in the synthesis of 1,1-diphenylethylene by reacting $Ph_3P{=}CH_2$ with benzophenone.[2] This work represents the birth of the olefination of aldehydes and ketones by phosphorus ylides, the Wittig reaction, which evolved into a reference synthetic method for the regio- and stereodefined construction of carbon−carbon double bonds.[3,4] Despite being intensively studied for almost 70 years, the mechanism of this fundamental transformation in organic synthesis is still under debate. In an excellent recent review, Gilheany and Byrne performed a detailed analysis of the experimental and computational studies about the mechanism of the Wittig reaction between phosphonium ylides and aldehydes or ketones.[5] Phosphorus ylides are categorized by the substituent(s) R attached to the ylidic carbon as nonstabilized (R = alkyl), semistabilized (R = alkenyl, phenyl), and stabilized (R = heteroatom-containing conjugating group, e.g., carbonyl, ester, nitrile, etc.). The accepted mechanism for the Li-salt free Wittig olefination of nonstabilized ylides under kinetic control involves a [2 + 2] cycloaddition to give a 1,2-oxaphosphetane intermediate (*cis*-**OPA**/*trans*-**OPA**, Scheme 1), which decomposes via the isomer formed by phosphorus pseudorotation to place the P−O bond in an equatorial position (*cis*-$\mathbf{OPA_{eq}}$/*trans*-$\mathbf{OPA_{eq}}$) followed by [2 + 2] cycloreversion to yield the olefin (*Z*-**OL**/*E*-**OL**), and a phosphine oxide (Scheme 1).[6,7]

In the absence of inorganic salts, the stereochemical course of the process can be explained through a combination of [1,2]-,[6,8] [1,3]-,[6] C−H···O,[4c,9] and dipole−dipole[9] interactions that control the relative energy of the transition states (*cis*-**TS**/*trans*-**TS**) of 1,2-oxaphosphetanes formation (Scheme 1). In a few cases, reversibility in this first step has been observed, and the *E*/*Z* selectivity obtained proceeds from the thermodynamic equilibrium between the diastereomeric oxaphosphetanes. This reversal of the cycloaddition step causes the so-called stereochemical drift.[10,11]

Special Issue: The New Golden Age of Organophosphorus Chemistry

Received: May 27, 2020

https://dx.doi.org/10.1021/acs.joc.0c01270
J. Org. Chem. XXXX, XXX, XXX−XXX

Scheme 1. Mechanism of Wittig Olefination[a]

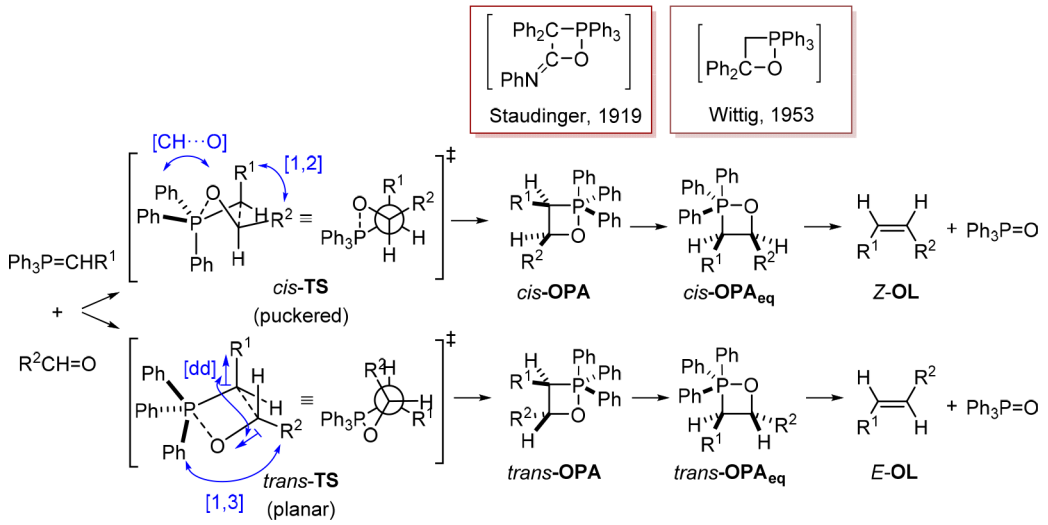

[a]Stereoelectronic interactions are highlighted in blue.

One hundred years after 1,2-oxaphosphetanes were first introduced,[1] they remain the only intermediates isolated in the Wittig reaction. Experimental evidence about the participation of 1,2-oxaphosphetanes in the Wittig olefination arise mostly from *in situ* NMR monitoring of the process at low temperatures.[10,12,13] Generally, 1,2-oxaphosphetanes are highly thermally labile species and are transformed into the corresponding olefin and P═O byproduct upon warming the NMR sample. A very small number of these intermediates have been isolated and structurally characterized through X-ray diffraction studies.[14] Representative examples are shown in Chart 1. Based on the origin of their thermal stability, they can be classified into two groups. Group A is formed by monoheterocyclic systems stabilized by strong electron-withdrawing substituents (e.g., **1**,[15] **2**,[16] and **3**[17]). Group B includes compounds characterized by the integration of the oxaphosphetane moiety into a polycyclic system. Spiro-compounds with rings connected through a pentacoordinated phosphorus atom seem to represent a particularly stable arrangement, as shown by the spiro-oxaphosphetanes **4**,[18] **5**,[19] and **6**.[20] The Martin ligand[21] (ML) and the *ortho*-benzamide ligand (*o*BA) proved to be very efficient scaffolds for OPA stabilization.[22,23] So far, only 1,2-oxaphosphetanes derived from nonstabilized ylides have been isolated as products of the Wittig reaction. It is nevertheless important to note that 1,2-oxaphosphetanes formally arising from ylides stabilized by a methoxycarbonyl group have been obtained through alkoxycarbonylation of stable precursors unsubstituted at C-3 (i.e., proceeding from nonstabilized ylides).[24]

Chart 1. Examples of 1,2-Oxaphosphetanes Characterized in the Solid-State with X-ray Diffraction[a]

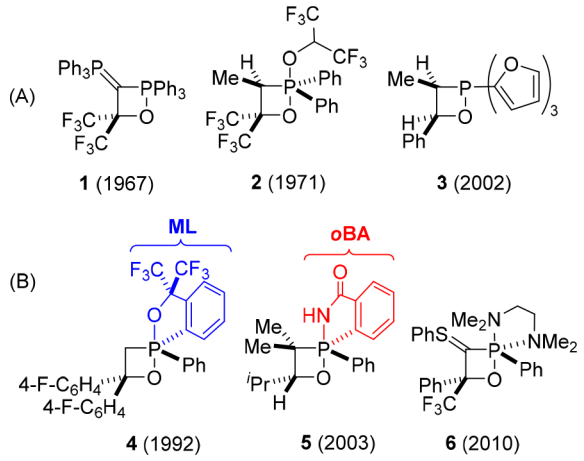

[a]Ligands ML and *o*BA are highlighted in blue and red, respectively.

Although most oxaphosphetanes isolated undergo olefination upon heating, the rather simple substitution pattern prevents gaining insight into the stereoelectronic effects that govern the reaction. We have previously shown that the stabilizing effect of the *o*BA ligand allowed us to obtain stable tri- and tetrasubstituted spiro-1,2-oxaphosphetanes **9** in a one-pot two-step process (Scheme 2).[19,23] First, double C_α and C_{ortho} deprotonation of phosphazene **7** with ^{t}BuLi at −90 °C provides dianion **8**,[25] which undergoes cyclocondensation at −35 °C by the attack of the ortho anion to the carbonyl group of the phosphazene moiety followed by the elimination of lithium methoxide to give the monoanionic intermediate **Li−I**. Then, the reaction of **Li−I** with aldehydes and ketones would afford lithiated species **Li−II**, which is converted into spiro-1,2-oxaphosphetanes **9** upon aqueous workup. The thermolysis of **9** in the toluene solution afforded the corresponding olefins **10** in a quantitative and stereospecific manner (Scheme 2).[19,23] In contrast to the accepted mechanism mentioned above,[5,26] the computational study of the thermal decomposition of **9** revealed that the [2 + 2] OPA cycloreversion to the corresponding alkenes **10** and benzoazaphospholone 1-oxide **11** is a single-step asynchronous reaction.[27] The positional interchange of apical and equatorial ligands around the phosphorus atom leading to an antiapicophilic P−O_{eq} OPA takes place along the reaction coordinate via mechanisms involving two (M_{B2}) or three (M_{B3}) and four (M_{B4}) Berry pseudorotations (BPR).[23] These mechanisms also explained the isomerization of OPA **9** into **9′** through inversion of the configuration of the phosphorus atom during thermal decomposition (Scheme 2).

In the light of the stability of spiro-compounds **9**, we reasoned that they could be used for investigating the stereoelectronic

https://dx.doi.org/10.1021/acs.joc.0c01270
J. Org. Chem. XXXX, XXX, XXX−XXX

Scheme 2. Synthesis of Spiro-1,2-oxaphosphetanes 9 and Alkenes 10

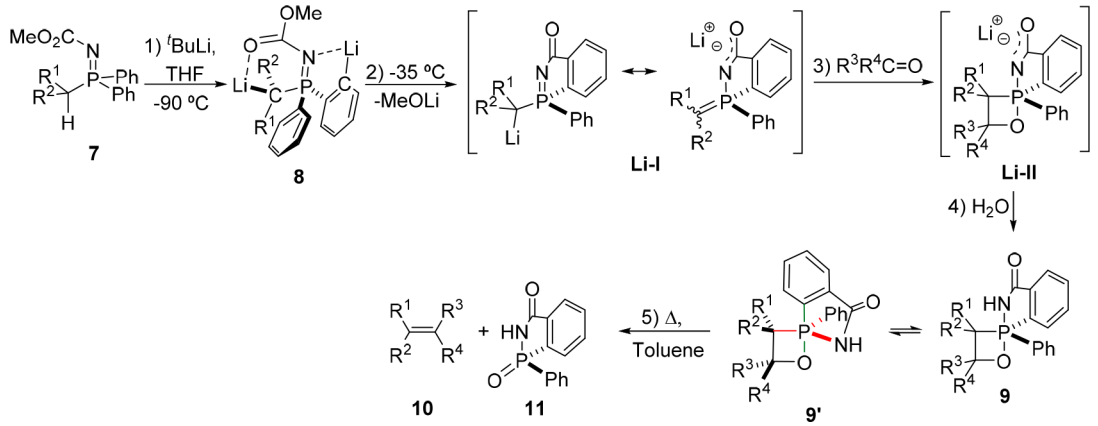

Table 1. Spiro-1,2-oxaphosphetanes 9 and 12 Synthesized and ^{31}P NMR Data, δ in ppm

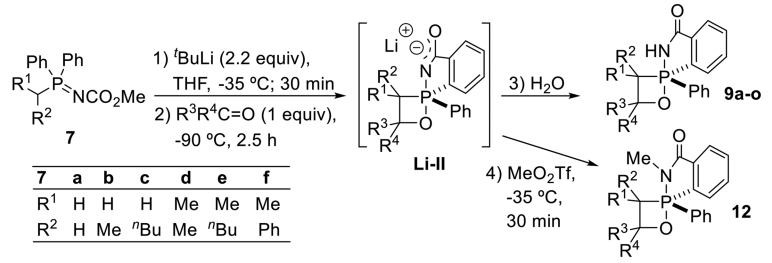

7	a	b	c	d	e	f
R^1	H	H	H	Me	Me	Me
R^2	H	Me	^{n}Bu	Me	^{n}Bu	Ph

Entry	Comp.	R^1	R^2	R^3	R^4	Trans:cis[a]	Conv. (%)	$\delta(^{31}P)$ Trans/cis[a]
1	**9a**	Me	Me	Me	Me		92	-63.9
2	**9b**	Me	Me	$CH_2(CH_2)_3CH_2$			93	-64.7
3	**9c**[b]	Me	Me	Ph	Ph		92	-65.5
4	**9d**[b]	Me	Me	Me	Ph		92	-65.5
5	**9e**[c]	Me	^{n}Bu	Me	Ph	76:24	65 (86)[d]	-66.6/-67.0
6	**9f**	Me	Me	*p*-F-C_6H_4	*p*-F-C_6H_4		93	-65.4
7	**9g**	Me	Me	*p*-Cl-C_6H_4	*p*-Cl-C_6H_4		95	-65.4
8	**9h**	Me	Me	*m*-CF_3-C_6H_4	*m*-CF_3-C_6H_4		97	-65.1
9	**9i**	Me	Me	*p*-Me_2N-C_6H_4	*p*-Me_2N-C_6H_4		88[e]	-64.2
10	**9j**[c]	Me	Me	H	*p*-MeO-C_6H_4	40:60	93	-65.0/-63.9
11	**9k**	Me	Me	H		51:49	96	-63.7/-63.6
12	**9l**[c]	Me	H	$CH_2(CH_2)_3CH_2$		5:95	82	-70.5/-73.4
13	**9m**	Me	H	Ph	Ph	3:97	89	-69.5/-72.4
14	**9n**	^{n}Bu	H	Me	Ph	0:100	87	-75.9
15	**9o**	Me	H	*p*-MeO-C_6H_4	*p*-MeO-C_6H_4	0:100	83	-72.8
16	**9p**	**Ph**	**Me**	**Me**	**Me**	**34:66**	**27**	**-68.3/-67.5**
17	**12a**	Me	Me	Me	Me		95	-53.4
18	*cis*-**12b**[a]	Me	H	Ph	Ph		87	-59.8
19	**12c**	Me	Me	Ph	Ph		95	-48.9
20	**12d**	Me	Me	*p*-MeO-C_6H_4	*p*-MeO-C_6H_4		91	-48.7

[a]Diastereomeric ratios determined through integration of the ^{31}P NMR spectra of the crude reaction mixture. The *trans*/*cis* descriptors indicate the relative orientation of the *P*-phenyl ring and the higher rank substituent linked either to C3 and/or C4 carbons of the oxaphosphetane ring. [b]Compound described in ref 23. [c]Compounds described in ref 25. [d]Reaction time with the ketone of 5 h. [e]Reaction time with the ketone of 5 h at a temperature of −35 °C.

features controlling olefin formation in the second step of Wittig olefination. Here we report the extension of the synthesis of *o*BA-stabilized spiro-oxaphosphetanes to the preparation of compounds with a substitution pattern that allows us to unravel the effects determining the course of the olefination process via thermolysis. New developments include the synthesis of *N*-alkylated derivatives and the isolation and structural characterization of the first example of a 1,2-oxaphosphetane derived from a semistabilized ylide derivative. Kinetic and thermodynamic parameters obtained in the olefination study revealed the influence of electronic and solvent effects as well as steric [1,2] and [1,3] interactions in the reaction pathway.

RESULTS AND DISCUSSION

Synthesis of *o*BA-Stabilized Spiro-1,2-oxaphosphetanes. Compounds **9** used in this study were prepared according to the procedure shown in Scheme 2 (Table 1).[25] Oxaphosphetanes **9a**−**p** were obtained in very high to excellent

https://dx.doi.org/10.1021/acs.joc.0c01270
J. Org. Chem. XXXX, XXX, XXX−XXX

yields, except for **9p** (see below). High yields of **9e** and **9i** were achieved by increasing the reaction time to 5 h (entry 5) and the reaction temperature to −35 °C (entry 9), respectively. Compounds **9c**,[23] **9d**,[23] **9e**,[25] **9j**,[25] and **9l**[25] reported previously have been included here in order to complete the kinetic studies and the analysis of the effects involved in the Wittig olefination. The reactions of phosphazenes **7b−c** monosubstituted at the *P*-C_α proceeded with excellent diastereoselectivity (cf. entries 12−15), whereas C_α-disubstituted phosphazenes **7d−e** provide oxaphosphetanes **9** with moderate to low diastereoselectivity (entries 5, 10, and 11). Diastereoisomers were separated by precipitation from diethyl ether or by column chromatography. All compounds were structurally characterized based on their spectroscopic data (Supporting Information). The stereochemistry was assigned through selective 1D gNOESY experiments. Recrystallization of oxaphosphetane *cis*-**9d** from a mixture of dichloromethane-hexane afforded single crystals suitable for X-ray diffraction analysis. The crystal structure is shown in Figure S13 (Supporting Information). Oxaphosphetanes *cis*/*trans*-**9k** formed in the reaction of dilithiated **7d** with (−)-mirtenal ((−)-(1*S*,5*R*)-6,6-dimethylbicyclo[3.1.1]-2-hept-en-2-carbaldehyde) are enantiomerically pure. Their configuration was assigned based on the 2D gNOESY spectra. This structural study showed that the racemic phosphazenyl carbanion added to the carbonyl group of (−)-mirtenal exclusively through the *si* face. Isomer *trans*-**9k** was recrystallized from a mixture of dichloromethane−hexane, and the X-ray crystal structure was measured (Figure S14).

The reaction of benzylphosphazene **7f** deserves a particular comment (Scheme 3). The phenyl ring attached to the P-CH

Scheme 3. Synthesis of Spiro-1,2-oxaphosphetane 9p

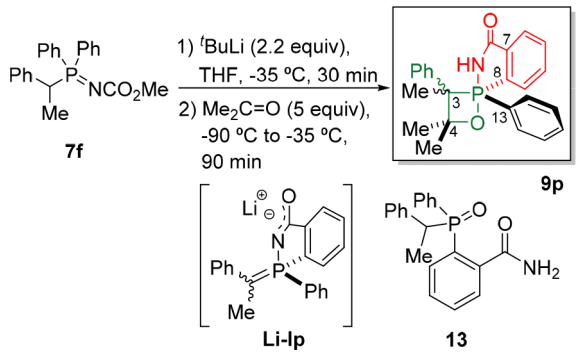

carbon means that this substrate will be the precursor of a semistabilized phosphorus ylide derivative (species **Li−I** in Scheme 2). Under the reaction conditions shown in Table 1 and using acetone as a carbonyl component, spiro-OPA *cis*- and *trans*-**9p** were obtained with 17% conversion together with a large amount of starting material (26%) and a number of byproducts (57%) (Scheme 3). After some experimentation, we found that the cleanest reaction leading to **9p** consisted of performing the double deprotonation in the standard manner followed by the addition of 5 equiv of acetone at −90 °C and allowing the temperature to rise to −35 °C for 90 min.

In this way, oxaphosphetanes *cis*-/*trans*-**9p** were obtained in a conversion of 27% and a ratio of 66:34 (Table 1) together with unreacted **7f** (38%) and the phosphorylbenzamides **13** (35%, mixture of two diastereoisomers in a ratio of 14:21) (Figure S1, Supporting Information). The formation of significant amounts of byproducts **13** arising from the hydrolysis of the lithiated cyclization intermediate **Li-Ip** is in agreement with the suggested reduction in nucleophilic reactivity of **Li-Ip** toward the carbonyl group of acetone.

Purification through two consecutive column chromatographies provided a small amount (2.6 mg, yield 1%) of nearly pure *cis*-**9p**, enough to achieve the structural characterization through mass spectrometry and spectroscopic methods. The HRMS spectrum showed the $[M + H]^+$ ion at m/z 390.1639 in agreement with the molecular formula of protonated **9p** ($C_{24}H_{25}NO_2P$ calculated exact mass: 390.1623). The ^{31}P NMR spectrum shows a resonance at δ −67.5 ppm in the expected range for a pentacoordinated phosphorus atom (Figure S2d). The ^1H and ^{13}C NMR spectra present the same pattern of signals of the family of compounds **9** (Figure S2a,c). The relative configuration of the P and C stereogenic centers was established based on 1D NOE experiments (Figure S2b). To the best of our knowledge, this is the first example of a 1,2-oxaphosphetane isolated from a semistabilized phosphorus ylide having a phenyl group at the ylidic carbon. It should be noted that Vedejs and Fleck reported the observation through ^{31}P NMR of C3-vinyl substituted OPAs stabilized by a dibenzophosphole system.[6c]

Spiro-oxaphosphetanes **9** contain an N−H bond that might participate in the olefination reaction via hydrogen bonding with the solvent, the phosphorus byproduct, or through self-association. To eliminate these possible contributions to the olefination process, we sought to prepare *N*-methylated derivatives of **9**. Quenching the lithiated species **Li−II** with methyl trifluoromethanesulfonate (MeOTf) at −35 °C during 30 min furnished *N*-methyl spiro-oxaphosphetanes **12** in excellent yields (Table 1, entries 17−20). *N*-Methylation is evidenced by the ^1H NMR spectra. Recrystallization of **12a** from hexane afforded a crystal suitable for X-ray diffraction analysis. The structure obtained is shown in Figure S15. A brief analysis of the main solid-state structural features of compounds *cis*-**9d**, *trans*-**9k**, and **12a** is given in the Supporting Information. The synthesis of **12** illustrates the wide scope of the methodology developed for the preparation of spiro-1,2-oxaphosphetanes making feasible the derivatization of the spiranic system in a one-pot manner. Furthermore, the *N*-methylated *o*BA ligand (M*o*BA) of **12** introduces new interactions with the substituents at carbon C3 of the oxaphosphetane ring, which will be analyzed below.

Synthesis of Olefins by Thermolysis of Spiro-1,2-oxaphosphetanes. Spiro-1,2-oxaphosphetanes **9** undergo a quantitative transformation into the corresponding alkenes **10** and benzazaphospholone **11** by heating in DMSO-d_6 at 140 °C overnight in an NMR tube (Table 2). *E*/*Z* isomerization was not observed during the NMR monitoring process; i.e., the stereochemical drift did not take place. Pure alkenes were obtained by dissolving the DMSO solution into CH_2Cl_2, washing with water followed by solvent elimination *in vacuo*. The addition of hexane to the crude reaction mixture dissolved the olefin and induced the quantitative precipitation of **11**. No signal was detected in the ^{31}P NMR spectrum of the hexane solution. Finally, solvent evaporation afforded pure tri- and tetrasubstituted alkenes **10**. The configuration of the carbon−carbon double bond was assigned based on the NOEs detected in 1D gNOESY spectra. Changes in the phosphorus configuration[28] could be unraveled by investigating the olefination of enantiomerically pure compounds *cis*-**9k** and *trans*-**9k** (Table 2). Although their thermolysis led to an alkene devoid of geometrical isomers, the benzazaphosphole **11** generated is chiral and arises from an enantiomerically pure

https://dx.doi.org/10.1021/acs.joc.0c01270
J. Org. Chem. XXXX, XXX, XXX−XXX

Table 2. Alkenes 10 Obtained by Thermolysis of Oxaphosphetanes 9 and 12c[a]

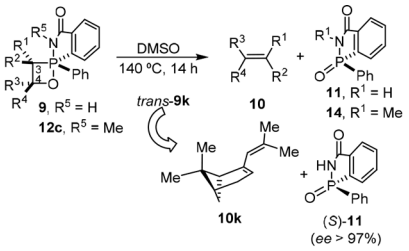

Entry	9	10	R^1	R^2	R^3	R^4
1	**a**	**a**	Me	Me	Me	Me
2	**b**	**b**	Me	Me	$CH_2(CH_2)_3CH_2$	
3	**c**	**c**[b]	Me	Me	Ph	Ph
4	*cis*-**d**	**d**	Me	Me	Me	Ph
5	*trans*-**e**	*E*-**e**	^{n}Bu	Me	Me	Ph
6	*cis*-**e**	*Z*-**e**	Me	^{n}Bu	Me	Ph
7	*trans*-**j**	**j**	Me	Me	H	*p*-MeO-C_6H_4
8	*trans*-**k**/*cis*-**k**	**k**	Me	Me	H	
9	*cis*-**l**	**l**	H	Me	$CH_2(CH_2)_3CH_2$	
10	*cis*-**m**	**m**	H	Me	Ph	Ph
11	*cis*-**n**	*Z*-**n**	H	^{n}Bu	Me	Ph
12	*cis*-**o**	**o**	H	Me	*p*-MeO-C_6H_4	*p*-MeO-C_6H_4
13	*cis*-**p**	**d**	Me	Ph	Me	Me

[a]Alkenes have been labeled with the same alphabetical identifier of the oxaphosphetane precursor. [b]The same alkene is formed in the thermolysis of **12c**.

oxaphosphetane with a phosphorus atom of (*R*) and (*S*) configuration, respectively.[29] Heating *cis*-**9k** at 130 °C in DMSO for 6 h afforded **10k** and **11** quantitatively. Chiral HPLC analysis of **11** showed an enantiomeric ratio (*R*)-**11**/(*S*)-**11** of 76:24 (Figure S3, based on the known absolute configuration of (*S*)-**11**).[23] Clearly, stereomutation occurred during fragmentation of the oxaphosphetane ring, causing partial racemization of **11**. This P-isomerization during olefination has been previously ascertained in *o*BA-stabilized OPAs.[23] Interestingly, the analogous reaction of *trans*-**9k** provided enantiomerically pure **11** (Figure S3). This means that, for this isomer, the reaction takes place stereospecifically without apparent stereomutation of the phosphorus atom.

The thermal decomposition of the *N*-methylated oxaphosphetane **12c** proceeded in an analogous manner to that of compounds **9**, affording alkene **10c** and *N*-methyl benzazaphospholone **14** quantitatively.

Kinetic Study of the Thermolysis of Spiro-1,2-oxaphosphetanes. To gain insight into the factors determining the energy profile of the second step of the Wittig reaction, we carried out a kinetic study of the thermolytic fragmentation of **9**/**12c**. The study was aimed at establishing relationships among the factors contributing to the relative stability of the ground state (GS) and transition state (TS) of the olefination with kinetic and thermodynamic data of the transformation. The substituents in the compounds selected may influence the reaction course through electronic effects, [1,2]/[1,3] steric interactions, and hydrogen bonding. Solvent effects were evaluated by measuring olefination rates in DMSO, DMF, and toluene. These effects are indicated using a color key in Chart 2. The TS shown in Chart 2 is that considered more representative of the olefination reaction (see computational section).[5,9,23]

[1,2] Interactions may be observed between C3/C4 and C3/P substituents. The asymmetric phosphorus atom of **9**/**12c** would lead to two different C3/P-[1,2] interactions labeled as C3/P_N-[1,2] and C3/P_{Ph}-[1,2]. The subscript designates the P-group syn to a C3 substituent. Substituents in C4/P would give rise to [1,3] interactions. A distinguishing feature of compounds **9**/**12c** is the much higher thermal stability as compared with 1,2-oxaphosphetanes generated in standard Wittig processes. Since substituents in C3 and C4 of **9**/**12c** are commonly found in Wittig reactions, their stability, i.e., the difficulty of olefination, must arise from the destabilization of the TS produced by spiranization. Taking into account that the consensus mechanism of olefination involves stereomutation of the phosphorus atom, the TS of the formation of alkenes **10** will be destabilized by three effects: the presence of two electronegative substituents in equatorial sites of a trigonal bipyramidal phosphorus (tbp, antiapicophilic element effect), the ring constrains arising from the five-membered ring (ring effect distortion of tbp), and the steric interaction generated by the NR^5 moiety eclipsed with one substituent in C3. These features make the decomposition of spiro-oxaphosphetanes **9**/**12c** the rate-determining step in the synthesis of alkenes **10**.

The kinetic of olefination was monitored through ^{31}P NMR spectroscopy. A known amount of **9**/**12c** was heated in the selected solvent, and ^{31}P NMR spectra were acquired at set time intervals. Monitoring the integrals of the upfield signal typical of oxaphosphetanes **9**/**12c** (δ in the range −65 to −75 ppm) and the peak at δ 20.5 ppm corresponding to **11** (in DMSO-d_6) afforded the concentration of each species as a function of time. The reaction showed a first-order dependence in the oxaphosphetane, as established by standard methods. The rate constants measured are summarized in Table 3 (for details, see Table S1). The error associated with the measurement of k is considered to be ≤2%.[30]

Rate differences will be determined by the balance of electronic and steric effects in the TS in the spiranic system. An overview of these effects is given in Chart 2. Based on atom electronegativities, C3 and C4 atoms in **9**/**12c** will bear a negative and positive partial charge, respectively, in the GS.

These charges are expected to increase in the TS of olefination due to the rupture of C3−P and C4−O bonds. This implies that electron-donating substituents in C3/C4 will destabilize/stabilize more the TS than the GS. In the reaction pathway, the hybridization of C3/C4 changes from sp^3 to sp^2. As a result, the C3−C4 bond distance would shorten, producing larger [1,2] interactions in the TS. This effect may be partially compensated by the increase of bond angles undergone by C3/C4. On the other hand, the C3−P bond is larger in the TS. Therefore, the substituents will move away from each other, contributing to the stabilization of the TS. However, due to phosphorus stereomutation, the C3 and P substituents become eclipsed in the TS, inducing strong [1,2] interactions. Simultaneously, the reordering of C3 and P substituents in the TS bring closer those linked to C3 and N, which gives rise to large destabilizing [1,2] interactions. [1,3] Steric effect between C4/P substituents also arises from two opposite contributions. Crowding will be

https://dx.doi.org/10.1021/acs.joc.0c01270
J. Org. Chem. XXXX, XXX, XXX−XXX

Chart 2. Spiro-1,2-oxaphosphetanes Selected for Thermal Decomposition Studies

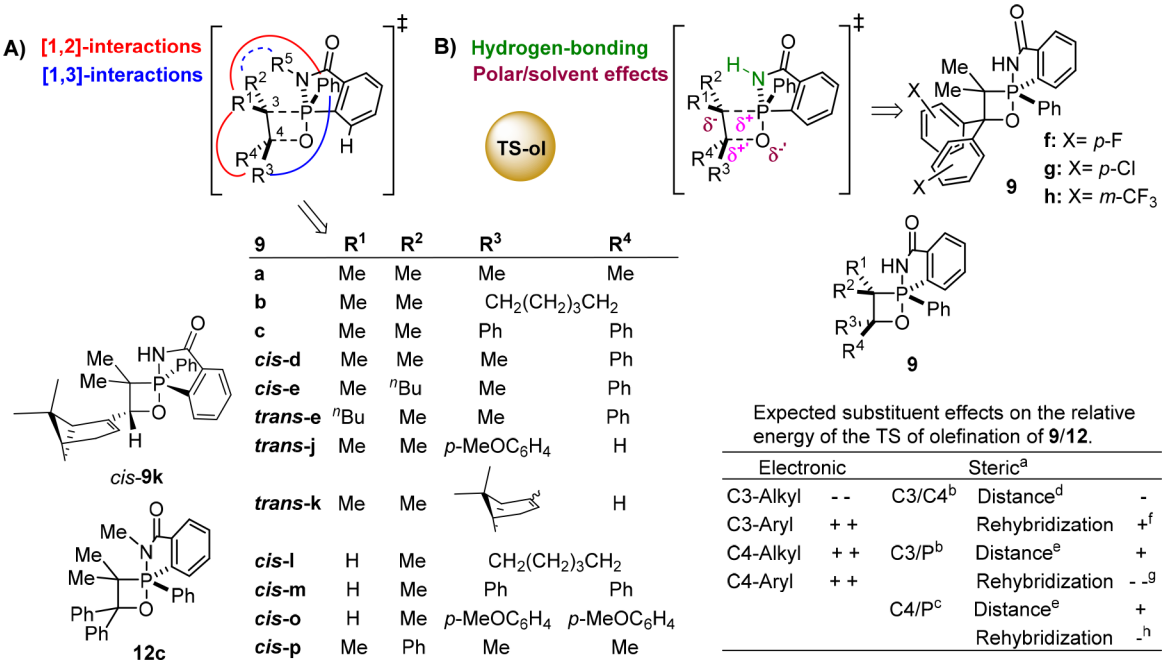

9	R^1	R^2	R^3	R^4
a	Me	Me	Me	Me
b	Me	Me	$CH_2(CH_2)_3CH_2$	
c	Me	Me	Ph	Ph
***cis*-d**	Me	Me	Me	Ph
***cis*-e**	Me	^{n}Bu	Me	Ph
***trans*-e**	^{n}Bu	Me	Me	Ph
***trans*-j**	Me	Me	*p*-$MeOC_6H_4$	H
***trans*-k**	Me	Me		H
***cis*-l**	H	Me	$CH_2(CH_2)_3CH_2$	
***cis*-m**	H	Me	Ph	Ph
***cis*-o**	H	Me	*p*-$MeOC_6H_4$	*p*-$MeOC_6H_4$
***cis*-p**	Me	Ph	Me	Me

Expected substituent effects on the relative energy of the TS of olefination of **9**/**12**.

Electronic		Steric[a]		
C3-Alkyl	- -	C3/C4[b]	Distance[d]	-
C3-Aryl	+ +		Rehybridization	+[f]
C4-Alkyl	+ +	C3/P[b]	Distance[e]	+
C4-Aryl	+ +		Rehybridization	- -[g]
		C4/P[c]	Distance[e]	+
			Rehybridization	-[h]

[a]As compared with the GS. Stabilization or destabilization of TS is indicated by a + or − sign, respectively. [b][1,2] Interactions. [c][1,3] Interactions. [d]Decrease in the TS. [e]Increase in the TS. [f]Distance between substituents is expected to increase. [g]Substituents eclipsed. [h]Distance between substituents is expected to decrease.

relieved in the TS through the increase in the distance between these atoms, whereas the C4/P geometrical reordering would destabilize the TS by slightly approaching the respective substituents. In the following, a qualitative analysis aimed at identifying major contributions to the rate of olefination of compounds shown in Table 3 is provided. Spiro-oxaphosphetanes **9**/**12** can be clustered in three groups according to the number and position of the substituents in the four-membered ring. With the exception of *cis*-**9p** (see below), the thermal stability increases in the series trisubstituted−C3-H (group I) ≪ trisubstituted−C4-H (group II) ≈ tetrasubstituted (group III). The fact that trisubstituted OPAs showing one proton at carbon C3 (entries 7, 8, and 9) olefinate significantly faster than those with the proton at carbon C4 (entries 10, 11, and 12) indicates that the thermal stability is primarily determined by C3/P-[1,2] interactions. The eclipsed arrangement of the substituents on the C3 and P atoms of the TS of olefination (**TS-ol**) would produce an increase of the energy barrier of decomposition. In agreement with this finding, **12c** showed the lowest rate of olefination (entry 14). In the **TS-ol**, the *N*-Me group would be very close to the neighbor C3-Me substituent, leading to very large C3/P-[1,2] steric interactions. Within OPAs of group I, the faster olefination of *cis*-**9o** with respect to *cis*-**9m** (factor 4.4, entries 8 and 9) may be attributed to the stabilizing charge effect of the methoxi groups in **TS-ol**-*cis*-**9o**.[31] The comparison with *cis*-**9l** is less evident. The restricted mobility of the cyclohexyl moiety would produce less C3/C4-[1,2] steric interactions than the C4-aryl groups of the other member of the group. In addition, the rehybridization of C4 in **TS-ol**-*cis*-**9l** would cause a relief of [1,3] diaxial interactions involving the C4−O bond. These features seem to accelerate the olefination of *cis*-**9l** slightly when compared with *cis*-**9o** (factor 1.15 at 80 °C in DMSO, Supporting Information). Concerning group II, the differences in the rate of olefination of *cis*-**9k** and *trans*-**9k** reveal changes in C4/P-[1,3] interactions (entries 11 and 12). The thermolysis of the trans isomer proceeded 1.28 times faster than the cis derivative, which suggests that the *P*-phenyl substituent gives rise to a larger [1,3] steric hindrance than the *o*BA moiety, thus destabilizing the TS of *cis*-**9k** with respect to *trans*-**9k**.

OPAs of group III that differ in the substitution pattern at C3 include *cis*-**9d**, *cis*-**9e**, and *trans*-**9e** (entries 4, 5, and 6). The olefination of *trans*-**9e**, 1.94 times faster than its C3-epimer *cis*-**9e** (Table 3, entries 5, 6), reflects the larger destabilization of **TS-ol**-*cis*-**9e** due to stronger C3/C4- and C3/P-[1,2] interactions; i.e., [1,2] steric hindrance arising from the *P*-phenyl substituent is also larger than that of *o*BA. *cis*-**9d** underwent the slowest decomposition in this subgroup (2.04 times slower than *cis*-**9e**), which points to a larger C3/C4- and C3/P-[1,2] steric strain in **TS-ol**-*cis*-**9d** compared with the **9e** derivatives. The rates of olefination of OPAs of group III bearing different substituents at C4 increase in the series *cis*-**9d** < **9c** < **9a** < **9b** (entries 1−4). These results show that the change of alkyl groups at C4 by phenyl substituents increases the energy barrier of olefination. This implies that destabilizing steric [1,2]- and [1,3] steric interactions in **TS-ol** of **9c** and *cis*-**9d** outweigh the electronic stabilization provided by the phenyl rings. Differences between *cis*-**9d**/**9c** and **9a**/**9b** can be ascribed to better charge delocalization in **TS-ol**-**9c** and to lower steric hindrance of the cyclohexyl ring compared with two methyl substituents (see above), respectively.

The fastest olefination is observed for *cis*-**9p** (entry 13). The decrease of C3/C4-[1,2] involving the C3-phenyl ring of **TS-ol**-*cis*-**9p**, owing to the increase of distances with the nearby substituents, together with the delocalization of the negative charge developed on C3 (Chart 2), will promote a large stabilization of the **TS-ol** of *cis*-**9p**. The easy decomposition of *cis*-**9p**, an OPA derived from a semistabilized phosphorus ylide, allows us to understand the difficulty in isolating this type of

https://dx.doi.org/10.1021/acs.joc.0c01270
J. Org. Chem. XXXX, XXX, XXX−XXX

Table 3. Rate Constants for Thermal Decomposition of Oxaphosphetanes Shown in Chart 2

Entry	Compound		k (s^{-1}) DMSO-d_6	Toluene-d_8	DMF-d_7	T (°C)
1	**9a**	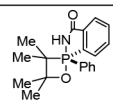	3.75(3) x10^{-4}			140
			1.57(2) x10^{-4}			130
2	**9b**	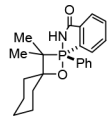	6.10(12) x10^{-4}		7.04(1) x10^{-4}	140
			2.9(6) x10^{-4}			130
3	**9c**	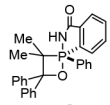	0.98(2) x10^{-4}	(3.82 x10^{-4})[a]		140
			4.05(8) x10^{-5}[b]			130
4	*cis*-**9d**	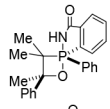	1.80(4) x10^{-5}			130
5	*cis*-**9e**	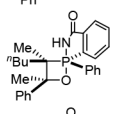	3.68(7) x10^{-5}			130
6	*trans*-**9e**	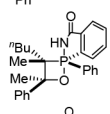	7.13(14) x10^{-5}			130
7	*cis*-**9l**	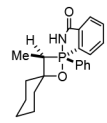	1.85(4) x10^{-4}	7.80(16) x10^{-4}		70
8	*cis*-**9m**	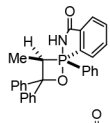	8.77(18) x10^{-5}			80
9	*cis*-**9o**	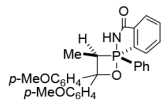	3.87(94) x10^{-4}			80
10	*trans*-**9j**	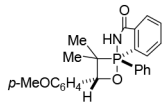	5.5(6) x10^{-5}	5.0(1) x10^{-6}[c]		130
11	*cis*-**9k**	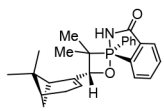	0.70(1) x10^{-4}			130
12	*trans*-**9k**	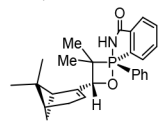	0.90(2) x10^{-4}			130
13	*cis*-**9p**	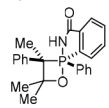	2.7(1) x10^{-3}[b]			130
14	**12c**	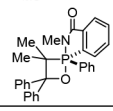	1.08(2) x10^{-4}		0.91(2) x10^{-4}	160
			0.43(1) x10^{-5}			130

[a]Calculated from the activation parameters in ref 23. [b]Calculated from the activation parameters. [c]Determined at 110 °C.

Wittig intermediates and the important stabilizing effect of the *o*BA ligand.

To summarize, in the absence of C3-aryl substituents, large C3/P-[1,2] steric interactions determine the high stability of spiro-oxaphosphetanes. The *P*-phenyl substituent gives rise to larger [1,2] and [1,3] steric hindrance than the *o*BA moiety. Charge delocalization at C4 stabilizes the TS of olefination, although less efficiently than the destabilization caused by [1,2] and [1,3] steric interactions. In *cis*-**9p**, the phenyl group at C3 that makes both steric and electronic effects would contribute to the stabilization of **TS-ol**, favoring a large decrease in the barrier of olefination.

https://dx.doi.org/10.1021/acs.joc.0c01270
J. Org. Chem. XXXX, XXX, XXX−XXX

The kinetic measurements for representative members of tri- and tetrasubstituted spiro-oxaphosphetanes have been performed at different temperatures, and the graphic representation of $\ln(k/T)$ as a function of $(1/T)$ (Eyring plot) afforded straight lines from which the activation parameters $\Delta H^{\ddagger}$ and $\Delta S^{\ddagger}$ were calculated (Table 4). Using these values, the Gibbs free energy of activation $\Delta G^{\ddagger}$ for each reaction at a given temperature was calculated. Interestingly, the process involves predominant negative entropic contributions both in the tri- and tetrasubstituted series of OPAs and $\Delta G^{\ddagger}$ increases in the series: *cis*-**9l** < *cis*-**9m** < *cis*-**9p** < **9b** < **9a** < **9c** < **12c**. The data collected in Table 4 allow for establishing the dominant role of C3/P_{Ph}-[1,2] interactions over other steric effects in the Wittig olefination of spiranes **9**/**12**.

Table 4. Activation Parameters of Selected Spiro-oxaphosphetanes in DMSO-d_6

Entry	Comp		$\Delta H^{\ddagger}$ (kcal·mol^{-1})	$\Delta S^{\ddagger}$ (e.u.)	$\Delta G^{\ddagger}_{403.15\ K}$ (kcal·mol^{-1})
1	**9a**		30.3 ± 0.5	-1.5 ± 1.2	30.9 ± 1.0
2	**9b**	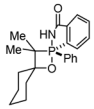	28.5 ± 1.3	-4.7 ± 3.1	30.4 ± 2.5
3	**9c**		29.2 ± 1.7	-6.8 ± 4.0	32.0 ± 3.3
4	*cis*-**9l**	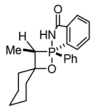	23.1 ± 1.5	-8.8 ± 4.3	26.6 ± 3.2
5	*cis*-**9m**		25.7 ± 0.1	-4.7 ± 0.2	27.6 ± 0.1
6	*cis*-**9p**		30.0 ± 3.6	3.7 ± 6.9	28.6 ± 6.3
7	**12c**	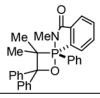	36.4 ± 1.3	6.8 ± 3.1	33.7 ± 2.6

The $\Delta G^{\ddagger}$ values of compounds dimethylated in C3 are 3.8−4.4 kcal mol^{-1} larger than those of C3-monomethylated analogues, cf. **9b**/*cis*-**9l**, **9c**/*cis*-**9m** (entries 2/4 and 3/5). This $\Delta\Delta G^{\ddagger}$ represents roughly the contribution to the activation energy of the olefination of a C3-methyl group cis to the *o*BA ligand. The difference of 0.6 kcal mol^{-1} between the two values can be assigned to slight differences in the steric demand (C3/C4-[1,2] C4/P-[1,3]) of the pentamethylene moiety and the phenyl rings linked to C4. In contrast, changes in $\Delta G^{\ddagger}$ involving C3/C4-[1,2] and C4/P-[1,3]-interactions are in the range of 0.5−1.6 kcal mol^{-1} (cf. **9a**/**9b**, **9a**/**9c**, and **9b**/**9c**).

It must be remembered that an estimation of the role of C3/C4-[1,2] interactions in the decomposition process is complicated by the participation of opposed effects (Chart 2). In particular, elucidating the contribution to the energy of the TS associated with approaching/moving away the substituent in C3 and C4 due to the change of hybridization of these carbon atoms must await the computational section. The contribution to $\Delta G^{\ddagger}$ of C3/P_N-[1,2] interactions can be quantified by comparing the values of **9a** and **12c** (entries 1 and 7). *N*-Methylation produced an increase of 1.72 kcal mol^{-1} of the activation energy barrier. Importantly, this larger $\Delta G^{\ddagger}$ of **12c** arises from an increase of the enthalpy of the reaction and a change in the sign of entropic contributions. The latter is now positive. Positive entropic effects are also responsible for the lower energy barrier of *cis*-**9p** with respect to **9a** ($\Delta\Delta G^{\ddagger}$ = 2.3 kcal mol^{-1}).

Solvent Effects. The solvent may influence the decomposition of **9** and **12** via polar and hydrogen-bonding interactions. These features were analyzed by measuring the rate of olefination of **9b**, **9c**, *cis*-**9l**, *trans*-**9j**, and **12c** in DMSO (ε = 46.45), DMF (ε = 36.71), and toluene (ε = 2.38) (Table 3, the kinetic study of **9c** in toluene has been previously reported[23]). Compounds **9c**,[23] *cis*-**9l**, and *trans*-**9j** olefinated significantly faster in the nonpolar solvent toluene than in the most polar solvent of the series, DMSO (entries 3, 7, and 10). A similar trend was observed for the rate of olefination of **9b** in DMF and DMSO. The reaction in the less polar solvent DMF took place at a slightly higher rate (factor 1.15, entry 2). The use of DMSO as a solvent increased $\Delta G^{\ddagger}$ of the thermolysis of **9c** in 1.1 kcal mol^{-1} with respect to the reaction reported in toluene (Table 4, entry 3).[23] Both $\Delta H^{\ddagger}$ and $\Delta S^{\ddagger}$ are lower in DMSO than in toluene. These results are consistent with a reaction whose TS is more polar than the GS. In this situation, the TS will be less efficiently solvated by toluene than by DMSO molecules (higher $\Delta H^{\ddagger}$) and will be less ordered ($\Delta S^{\ddagger}$ more positive). The lower $\Delta G^{\ddagger}$ value for the reaction in toluene would reflect the larger contribution of entropic factors to the process.

DMSO may affect the rate of olefination via polar and hydrogen-bonding interactions. The latter contribution will be absent in the thermolysis of **12c** lacking the NH group. In this case, olefination in DMSO proceeded 1.19 times faster than in DMF (Table 3, entry 14). This behavior can be explained by considering that in the absence of hydrogen bonding, the stabilization on the polar TS provided by the more polar solvent (decrease of $\Delta H^{\ddagger}$) will prevail over the entropic contributions due to less efficient solvation.

Stereomutation. Thermolysis of *cis*-**9e** and *trans*-**9e** provided the corresponding olefin together with a new spiro-oxaphosphetane (Figure S6). The products obtained as *cis*-**9e″** and *trans*-**9e″** are shown in Chart 3. Full details about the evolution of reaction products as a function of time are given in Table S2. A similar finding was observed previously for compounds *cis*-**9d** and *cis*-**9l**.[23]

The new compounds were identified *in situ* through NMR spectroscopic analysis as permutational isomers in which the configuration of the phosphorus atom is inverted with respect to the starting substrate. The relative configuration was established based on 1D gNOESY spectra (Figure S7). The highest amount of *P*-stereoisomers were obtained for the ratios *cis*-**9e**/*cis*-**9e″** of 34.8:21.7 and *trans*-**9e**/*trans*-**9e″** of 28.2:9.1 (Table S2). Importantly, alkenes *Z*-**10e** and *E*-**10e** were obtained without traces of products of geometrical isomerization being detected. The retention of the C3/C4 configuration during thermolysis confirms that the new oxaphosphetane formed must be an epimer of the starting compound at the phosphorus center.

Spiro-oxaphosphetanes **9** contain a pentacoordinated phosphorus atom with a tbp geometry. Isomerization may occur

https://dx.doi.org/10.1021/acs.joc.0c01270
J. Org. Chem. XXXX, XXX, XXX−XXX

Chart 3. (a) Oxaphosphetanes Formed by Stereomutation and (b) Mechanism of Berry Pseudorotation

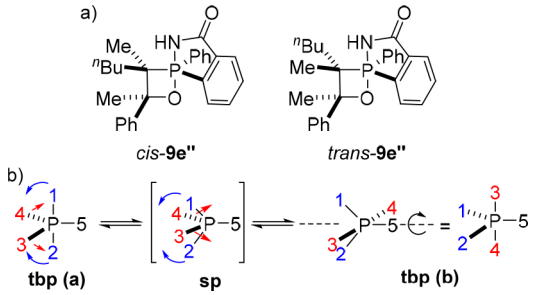

through sequential Berry pseudorotations[32] (MB1, MB2, MB3, MB4).[23,33] The process can be visualized in Chart 3 for a tbp with five different ligands. Defining ligand 5 as a pivotal center, the angle between apical positions 1 and 2 closes down with simultaneous opening up of the angle involving ligands 3 and 4. In this way, tbp (a) apparently rotates (pseudorotate) toward tbp (b) via a square pyramide (sp) intermediate.

Stereomutation in enantiomerically pure *cis*-**9k** implies that the byproduct **11** formed in the olefination reaction will be partially racemized. Moreover, the rates of olefination measured do not correspond to a single process. For the determination of the rate constants, we have considered that both isomers represent a single reagent. This assumption is compatible with two premises: the two pseudorotamers decompose through a common intermediate (Curtin−Hammett principle) or olefination proceeds through different intermediates of similar activation energies, affording average rate constants. Support for this latter assumption is provided by the relatively low concentration of permutational isomers detected and by the fact that fragmentation of *cis*-**9l** (70 °C), *cis*-**9e** (115 °C), and *trans*-**9e** (115 °C) in toluene took place without the formation of pseudorotamers. In all cases, the representation of $\ln[\mathbf{9}]_t$ against time originates straight lines of $r \geq 0.997$ (Supporting Information). The ^{31}P NMR monitoring of the olefination reactions showed that isomerization occurred in parallel with olefin formation (Figure S6, Table S2). Considering that stereomutation has been observed in most cases in which a new diastereoisomer could be formed, it is reasonable to assume that decomposition of spiro-oxaphosphetanes **9** at 130 °C involves, most probably, small contributions of phosphorus isomerization processes exchanging the positions of the two equatorial ligands.

Computational Study of the Olefination of Spiro-oxaphosphetanes. The results discussed above have revealed that the thermal decomposition of compounds **9** is a process characterized by a negative entropy, except for *cis*-**9p** and **12c**, and a polar transition state in which relative energy depends on a combination of electronic, steric, and solvent effects. Besides fragmentation, the pentacoordinated phosphorus undergoes stereomutation, causing partial racemization of the phosphorus center of some derivatives. In order to understand the stereoelectronic factors determining the olefination of spiro-oxaphosphetanes, we have performed a DFT study of the potential energy surface (PES) for the thermolysis of **9** and **12**. Three functionals were evaluated using the olefination of **9a** and **12c** as test reactions: B3LYP/6-31G*, M06/6-31G*, and M06-L/6-31G* M06-2X/6-31G*. The best results including London dispersion correction were obtained with M06-L/6-31G* (Tables S3 and S4), and therefore, this level of theory was applied to all calculations.[34] All stationary points located were characterized by computing the harmonic vibrational frequencies. In the case of the transition structures, the intrinsic reaction coordinate (IRC) calculations were performed in order to correlate the structures found with those of the starting reagents and the reaction products. The computations were carried out with the Gaussian09 program.[35] First, we completed the study of the thermochemistry of **9c** by computing the effect produced by changing the solvent of the decomposition reaction from toluene to DMSO. Next, the potential energy surface (PES) of the thermolysis of **12c** was investigated with the aim of explaining the higher stability of OPAs bearing the *m*BA ligand with respect to the *o*BA-stabilized derivatives. Then, [1,2] and [1,3] interactions were examined by calculating the energy profile of suitably substituted compounds **9** including **9a**, **9b**, **9c**, *cis*-**9m**, and **12c**.

We have previously shown that the thermal transformation of **9c** into alkene **10c** and benzoazaphosphole **11** could take place through two mechanisms, A and B (Scheme 4).[23] Route A is the

Scheme 4. Key Computational Results of the Olefination of 9c in the Gas Phase

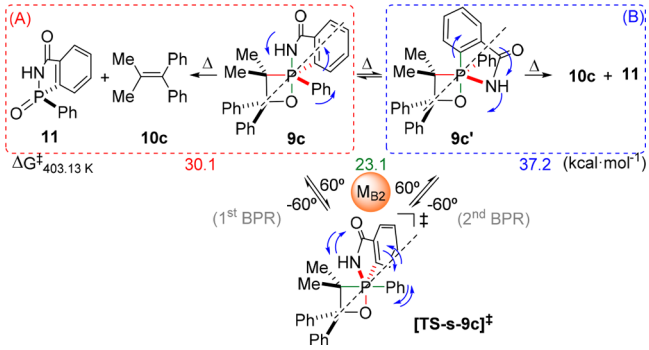

direct conversion of **9c** into products with an activation barrier of 30.1 kcal mol^{-1} (recalculated from B3LYP/6-31G* to the level of theory M06-L/6-31G*, Table S5, Figure S8) in excellent agreement with the experimental value of 30.9 kcal mol^{-1} determined in toluene as a solvent.[23] The formation of **9c** is a highly exothermic and irreversible reaction.

Route B is also a single-step process that starts with the permutational isomer **9c′** and proceeds to the products through a barrier of 37.2 kcal mol^{-1}; i.e., decomposition via channel A is highly favored ($\Delta\Delta G^{\ddagger}$ = 7.1 kcal mol^{-1}). The higher energy barrier of channel B correlates with the larger distortion of the geometry of **TS-ol-9c′** from an ideal tbp, defined by the deviation of the P atom (ΔP = 0.228) from the basal plane,[36] with respect to **TS-ol-9c** (ΔP = 0.213) (Figure S8). The antiapicophilic P−N_{eq} isomer **9c′** is formed by stereomutation of **9c** via an M_{B2} mechanism with a barrier of 23.1 kcal mol^{-1}. This barrier is 7 kcal mol^{-1} lower than the activation energy for olefination via channel A, which indicates that stereomutation of **9c** occurs faster than fragmentation.[13,28] This feature supports the observation of stereoisomers in the olefination of compounds **9** in which inversion of the configuration of the phosphorus atom originated a new diastereoisomer (Figure S7).

The single-step mechanism of decomposition of spiro-1,2-oxaphosphetanes **9c** and **9c′** implies that the process does not involve the formation of an intermediate OPA with C3 in the apical position.[27] Analogous results have been found previously in the theoretical study at the MP2 level of the Wittig reaction of

https://dx.doi.org/10.1021/acs.joc.0c01270
J. Org. Chem. XXXX, XXX, XXX−XXX

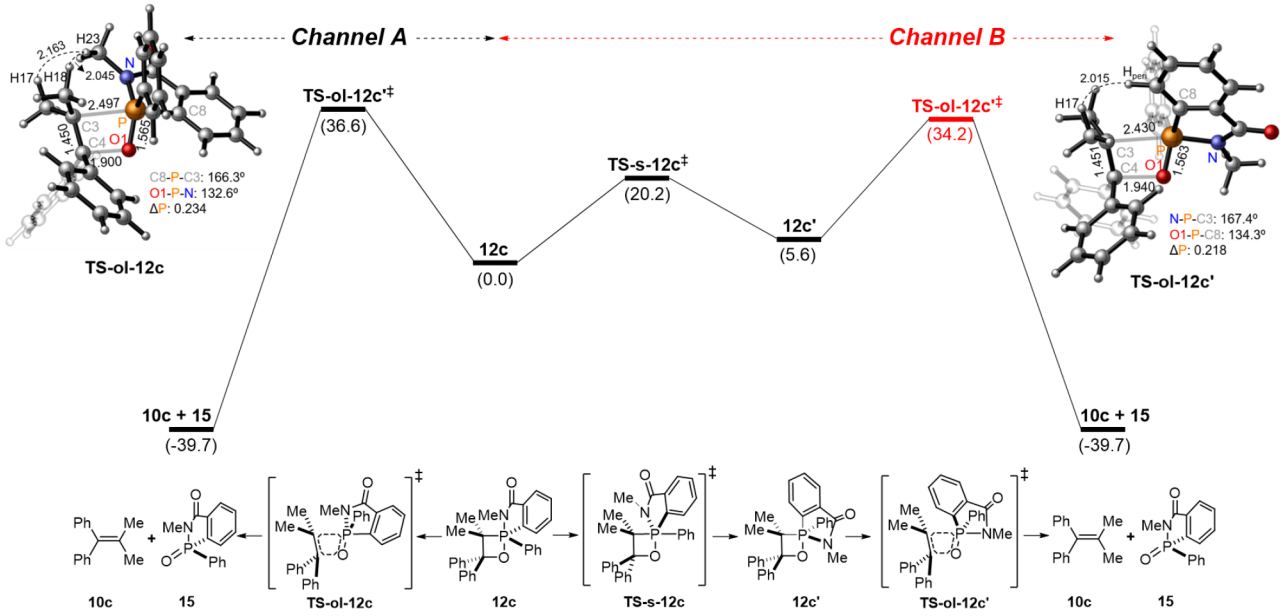

Figure 1. Potential energy surface of the thermal decomposition of **12c** at 130 °C calculated at the M06-L/6-31G(d) level of theory. Free energies (in brackets, kcal mol^{-1}) are relative to the starting materials.

very simplified model compounds.[37] Dynamic calculations on similar systems showed that stereomutation takes place almost without an energy barrier[38] or could not be detected.[39] Furthermore, the TS of olefination is more polar (μ = 4.1 D) than the starting spiro-oxaphosphetane (μ = 2.97 D), in agreement with the results of the kinetic study.

To complete this study, the macroscopic contribution of the solvent to the thermal decomposition of **9c** was estimated by using the SMD method of solvent interaction (Table S6).[40] The ΔG_{solv} values obtained as 30.0 and 31.6 kcal mol^{-1} for the reaction in toluene and DMSO, respectively, are in good agreement with those experimentally determined (Tables 3 and 4, entries 3) and support that the decomposition of **9c** takes place faster in toluene than in DMSO.

Theoretical Study of the Olefination of ***12c****.* Thermolysis of **12c** is characterized by the largest $\Delta H^{\ddagger}$ and $\Delta S^{\ddagger}$ measured, the latter being now positive. Similar to **9c**, the computational study of the olefination of **12c** at the M06-L/6-31G* level of theory led to seven stationary points: two spiro-oxaphosphetanes isomers, **12c** and **12c′**, the transition states of their stereomutation, **TS-s-12c**, and olefination, **TS-ol-12c** and **TS-ol-12c′**, and the reaction products **10c** and **15**. The energy profile is shown in Figure 1. Relative energies and thermodynamic parameters are given in Table S7. The stationary points located are qualitatively analogue to the corresponding structures calculated for the fragmentation of **9c** (Figures S9 and S10). Compound **12c** matches the isomer experimentally observed and is considerably more stable than the permutational isomer **12c′** ($\Delta\Delta G_{(12c-12c')}$ = 5.6 kcal mol^{-1} at 130 °C). This energy difference indicates that the equilibrium between both isomers is completely displaced to **12c**, thus explaining that this is the only stereoisomer experimentally observed.

12c/**12c′** stereomutation proceeds through an M_{B2} mechanism via the transition state **TS-s-12c**. Interestingly, the activation energy barrier of this process (20.2 kcal mol^{-1}) is 2.9 kcal mol^{-1} lower than that calculated for the isomerization of **9c** to **9c′** and significantly lower than the energy required for the olefin-forming reaction. Moreover, the presence of a methyl on the nitrogen shortens the energy gap between isomers **12c** and **12c′** in 0.3 kcal mol^{-1} as compared with **9c** and **9c′** (cf. Tables S5 and S7) and increases the energy liberated in the olefination reaction in 3.6 kcal mol^{-1} with respect to **9c**. The higher exothermicity of the decomposition of **12c** is a consequence of the destabilization of its GS with respect to **9c** due to the steric interaction of the N-Me group with the C3-methyl cis to the P-phenyl ring, a structural feature already evidenced in the X-ray structure of **12a** (Figure S15)

Most importantly, contrary to **9c**/**9c′**, olefination of **12c′** through channel B is energetically favored with respect to **12c** (channel A) by 2.4 kcal mol^{-1}. This energy difference implies that 95% of the molecules will olefinate via channel B. The destabilization of **TS-ol-12c** arises from the steric hindrance between the methyl groups linked to the nitrogen and to C3 (distortion of the tbp, ΔP = 0.234, Figure S9). This proximity effect is counterbalanced by a remarkable lengthening of the P−C3 bond distance (2.497 Å, Figure 1). In contrast, the N-Me group of **TS-ol-12c′** is located in a region devoid of relevant steric effects (ΔP = 0.218, Figure S10), and the structural parameters are very similar to those of the TS for the olefination of **9c′**. Therefore, the lower energy barrier calculated for channel B can be assigned to the loss of torsional strain in the transition state as compared with channel A, which correlates with the ΔP values computed. The large positive entropy of activation found for channel B supports this hypothesis. Furthermore, the $\Delta G^{\ddagger}$ = 34.2 kcal mol^{-1} calculated for olefination through channel B is in good agreement with that experimentally determined in DMSO (Table 4, entry 7). A few antiapicophilic P−O_{eq} OPAs have been isolated.[41] However, it has been shown that they convert into the P−O_{ap} isomer during thermal decomposition.[22a]

Analysis of Charge Effects. Next, we undertook the theoretical study of the stereoelectronic interactions involved in the olefination reaction. Charges distribution around the 1,2-oxaphosphetane ring in the olefination pathway were calculated at the NBO level for derivatives **9a**, **9c**, and *cis*-**9m**. The P and O heteroatoms show the expected behavior: higher charges in the transition state than in the ground state (Tables S8). Regarding

https://dx.doi.org/10.1021/acs.joc.0c01270
J. Org. Chem. XXXX, XXX, XXX−XXX

Table 5. Calculated (M06-L/6-31G*) Energies and Activation Parameters for the Transition States Found in the Study of [1,2] and [1,3] Interactions and Selected Bond Distances in Å[a]

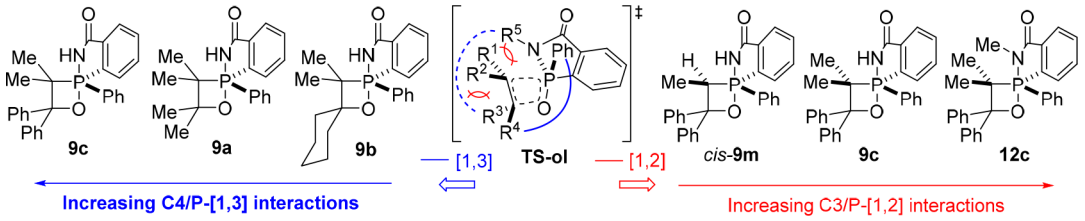

entry	structure	ΔE^b	$\Delta H^{\ddagger b}$	$\Delta S^{\ddagger c}$	$\Delta G^{\ddagger b}_{403.15\ K}$	P−C3	C4−O1	C3−C4	P−O1
1	**TS-ol-*cis*-9m**	28.9	27.5	0.3	27.4	2.254 (1.838)	1.998 (1.430)	1.428 (1.555)	1.559 (1.777)
2	**TS-ol-9c**	31.9	30.6	1.3	30.1	2.316 (1.855)	1.975 (1.423)	1.449 (1.576)	1.560 (1.778)
3	**TS-ol-9a**	30.2	28.7	0.6	28.5	2.362 (1.863)	1.961 (1.438)	1.435 (1.558)	1.556 (1.763)
4	**TS-ol-9b**	30.0	28.5	0.5	28.3	2.341 (1.85)	1.989 (1.442)	1.436 (1.558)	1.557 (1.761)
5	**TS-ol-12c′**	36.6	35.2	2.5	34.2	2.430 (1.877)	1.940 (1.424)	1.451 (1.570)	1.563 (1.786)

[a]Bond distances in the corresponding OPA ground state are indicated in brackets. [b]The reference structure is indicated by $\Delta E^{\ddagger}$, $\Delta H^{\ddagger}$, and $\Delta G^{\ddagger} = 0$ kcal mol^{-1}. [c]The reference structure is indicated by $\Delta S^{\ddagger} = 0$ e.u. (cal K^{-1} mol^{-1}).

C3 and C4, the TS of olefination of compounds **9** seems to be stabilized by dispersing the increase of negative/positive charge on C3/C4 through the respective substituents.

Analysis of [1,2] Interactions. The calculations above have shown that, in the transition state of the olefin-forming step, the substituents in carbon C3 and in the phosphorus atom are eclipsed. Therefore, increasing the size of the substituents around the P−C3 bond will destabilize the TS of the reaction. To complement the results obtained for **9c** and **12c**, we have extended the calculations to *cis*-**9m** (Figure S11). The different substitution patterns in C3 of these compounds will allow us to correlate differences in the thermodynamic parameters of olefination with steric [1,2] interactions. These may arise from the proximity of the substituents on C3 to those bonded to the phosphorus atom and to C4. Only the most favored pathway of olefination of OPAs stabilized by *o*BA (channel A) and M*o*BA (channel B) ligands was investigated. Energy parameters and bond distances relevant for the discussion are given in Table 5. The free energy calculated in the gas phase for the decomposition of *cis*-**9m** is in excellent agreement with experimental values obtained in the polar solvent DMSO (cf. entries 1/5 of Table 5/4).

Entries 1, 2, and 5 in Table 5 show some clear trends: (i) the reaction is highly asynchronous (in **TS-ol**, P−C3 and C4−O1 bond dissociations are notably more advanced than C3−C4 and P−O1 double bond formation), (ii) P−C3/C4−O1 bond distances increase/decrease by introducing Me groups at C3 (cf. **9c** and *cis*-**9m**, $\Delta_{P-C3}/\Delta_{C4-O1}$ = 0.062/−0.023 Å) and at the nitrogen atom (cf. **12c** and **9c**, $\Delta_{P-C3}/\Delta_{C4-O1}$ = 0.114/−0.035 Å). Therefore, the reaction reaches the **TS-ol** more and more later with an increasing number of methyl groups attached to C3 and N. Accordingly, $\Delta H^{\ddagger}$ and $\Delta S^{\ddagger}$ increase in the series *cis*-**9m** < **9c** < **12c** (**TS-ol** more product like, increase of disorder). Interestingly, this feature correlates with the increment of distortion of the tbp from the GS to the TS for the most favored olefination channel ($\Delta\Delta P$ = 0.107 (*cis*-**9m**, Figure S11), 0.119 (**9c**), 0.149 (**12c**)). The $\Delta G^{\ddagger}$ values given in Table 5 indicate that the introduction of a methyl group at C3 produced an increase of the energy barrier of olefination of 2.7 kcal mol^{-1}. This value is notably smaller than the contribution to $\Delta G^{\ddagger}$ of 4.4 kcal mol^{-1} experimentally observed in the polar solvent DMSO (entries 3 and 5, Table 4).

The calculations provide support to previous assumptions about the reasons for the stability of compounds **9** and the prevailing contribution of C3/P- vs C3/C4-[1,2] interactions to $\Delta G^{\ddagger}$. In **TS-ol**, the C3 and P substituents are eclipsed. The shortest distances are found for the C3-substituent and the NH in a mutual cis orientation (2.003/2.007 Å for *cis*-**9m**/**9c**, channel A, Table S9). They are lower than the sum of van der Waals radii (2.18 Å); i.e., along this series, **TS-ol** becomes more destabilized and $\Delta G^{\ddagger}$ olefination increases, in agreement with the experimental observations. For the *N*-methyl derivative **12c**, the strong C3-Me/NMe interactions determined that olefination through channel B involving the P−N_{eq} isomer **12′** became the preferred pathway of decomposition. During olefination, substituents in C3 and C4 cis to the *P*-phenyl group move away from each other, whereas those cis to the benzazaphosphole system come closer (Table S9). In any case, the changes in interatomic distances are much smaller than those observed for C3/P-[1,2] interactions. Hence, the stability of compounds **9**/**12** can be assigned to strong C3/P-[1,2] interactions in **TS-ol** with those involving the NH/NMe being the strongest.

C3/C4-[1,2] interactions are also present; however, they produce two opposing effects, and their contribution to $\Delta G^{\ddagger}$ of olefination seems to be significantly lower. Although the discussion above has been centered on steric effects, it must be remembered that electron-donating groups such as Me at a carbon, which develops a negative charge in the TS, will also contribute to increasing $\Delta G^{\ddagger}$ by destabilizing **TS-ol**.

Analysis of [1,3] Interactions. The kinetic study of substituents effect in C4 on the rate of olefination suggested that large groups in this carbon increased the energy barrier of the reaction due to [1,3] interactions with groups linked to the phosphorus atom. In this context, the contribution of the cyclohexyl moiety of **9b** to the rate of decomposition remains arguable. To clarify these uncertainties, we performed a theoretical study of the olefination of **9a**, **9b**, and **9c**, having different substituents in C4 (Figures S8, S11, and S12). The energies calculated for these transformations and some selected bond distances are given in Table 5 (entries 2−4). The olefination barrier increases in the series **9b** < **9a** < **9c**, in excellent agreement with the experimental results (Table 4).

The analysis of distances of the dissociating/forming bonds in **TS-ol** of the compounds under study revealed the existence of only very small differences, insufficient to explain the changes in

https://dx.doi.org/10.1021/acs.joc.0c01270
J. Org. Chem. XXXX, XXX, XXX−XXX

activation parameters shown in Table 5. Differences between **9a** and **9b** can be explained by analyzing steric effects between C4/P substituents. The C4-methyl group of cis geometry with the P-phenyl ring in the **TS-ol** of **9a** become much closer ($\Delta_{(Me19\cdots PhP)}$ = −0.423 Å) than the corresponding C4-CH_2 protons of the **TS-ol** of **9b** ($\Delta_{(CH219\cdots PhP)}$ = −0.136 Å) (Table S9) causing a larger destabilization of **TS-ol-9a** with respect to **TS-ol-9b** and, consequently, an increase of $\Delta G^{\ddagger}$ of olefination.

The replacement of methyl groups by phenyl substituents in C4 (cf. compounds **9a** and **9c**) introduces electronic effects together with [1,2] and [1,3]-interactions. NBO charge calculations indicate that the CPh_2 moiety delocalizes the positive charge developed in C4 of **TS-ol** more efficiently than the CMe_2 group (Table S8). In the same vein, when going from GS to **TS-ol** of **9c**, the C4-Ph and P-Ph groups move away (an increase of the distance of 0.075 Å), leading to less C4/P_{Ph}-[1,3] interactions. C3/C4-[1,2] interactions in **TS-ol** of **9a** and **9c** are destabilizing due to the approach of the substituents (e.g., change of distances for **9c** between substituents with a cis/trans geometry to the *P*-phenyl of −0.072/−0.049 Å). These effects suggest that, contrary to calculations and experimental observations, **9c** should olefinate faster than **9a** via a more stabilized **TS-ol**. The key difference proceeds from the C3/P_{NH}-[1,2] interactions. These are much stronger in **TS-ol-9c** due to a reduction of the Me···HN distance of 1.157 Å (vs 0.805 Å for **TS-ol-9a**, Table S9). The destabilization of **TS-ol** of **9c** caused by this steric effect explains that it shows the largest energy barrier of olefination on the series of compounds studied.

CONCLUSIONS

The reaction of C_{α},C_{ortho}-dilithiated phosphazenes with aldehydes and ketones represents the first general method of accessing to a large variety of air and temperature stable C3/C4 tri- and tetrasubstituted spiro-1,2-oxaphosphetanes stabilized by the *o*BA and M*o*BA ligands **9**/**12**. The wide scope of the process is supported by the synthesis of homochiral products using the aldehyde (−)-mirtenal as an electrophile and the isolation of the first example of a 1,2-oxaphosphetane derived from a semi-stabilized phosphorus ylide *cis*-**9p**. Stereoselectivities are generally excellent. Mixtures of stereoisomers were readily separated through column chromatography. Their thermolysis afforded the corresponding alkenes quantitatively and stereospecifically. In a number of cases, the permutational isomers by *P*-stereomutation could be structurally characterized *in situ* through NMR spectroscopy. The rates of olefination of **9**/**12** showed a dependence on stereoelectronic and solvent effects and decreased with an increasing number of substituents in C3/C4 and the nitrogen atom. The reaction is characterized by a negative $\Delta S^{\ddagger}$, except for *N*-methylated derivatives, involved a polar transition state, and proceeds faster in low polar solvents.

The computational study of the thermolysis of **9**/**12** showed that OPAs **9**/**12** olefinated via species (N, O)(Ph, C_6H_4, C)/(C_6H_4, O)(C, N, Ph) designated as "channel A" and "channel B", respectively. These processes are associated with the lowest distortion of the tbp in the respective TSs. *P*-Stereomutation takes place through an M_{B2} mechanism, which exchanged the apical nitrogen with the equatorial C_{ipso} carbon of the *o*BA/M*o*BA moiety. For both channels, the activation energy of olefination is higher than that of stereomutation. In contrast with the consensus mechanism of Wittig olefination, oxaphosphetane ring fragmentation occurred via a concerted asynchronous reaction (dissociation of P−C3 more advanced than that of C4−O1). The analysis of electronic, solvent, and steric effects on the activation energy supported the determining contribution of C3/P-[1,2] interactions to $\Delta G^{\ddagger}$ and the decrease of [1,3]-interactions in the TS of the reaction. This TS is more polar than the starting spiro-oxaphosphetane and showed a distorted tbp geometry with C3 and C8 in apical positions. The higher rate of decomposition observed in solvents of low polarity was a consequence of macroscopic solute−solvent interactions. The stabilization of 1,2-oxaphosphetane through *o*BA and M*o*BA ligands opens the way to the isolation of elusive intermediate species in the Wittig reaction making feasible their structural and thermochemical characterization. Work is underway to extend the applications of *o*BA and M*o*BA ligands.

EXPERIMENTAL SECTION

General Information. Melting points were measured on a Büchi B-540 capillary melting point apparatus. High-resolution mass spectra were recorded on Acquity UPLC-Xevo QtoF (Waters) equipment using positive electrospray ionization (ESI). NMR spectra were acquired on a Bruker Avance III HD 300 (^{1}H 300.13 MHz; ^{13}C 75.47 MHz; ^{19}F 282.40 MHz; ^{31}P 121.49 MHz) and a Bruker Avance III HD 500 (^{1}H 500.13 MHz; ^{13}C 125.76 MHz; ^{31}P 202.46 MHz) at room temperature using $CDCl_3$ as a solvent. Chemical shifts are referred to internal tetramethylsilane for ^{1}H and ^{13}C, internal CCl_3F for ^{19}F, and external 85% H_3PO_4 for ^{31}P. The enantiomeric excesses were determined by HPLC analysis on an HP1100 instrument using a Chiralcel OD-H (5 μm, 150 × 4.6 mm) column and a diode array detector.

Reactions involving organolithium reagents were performed under an inert atmosphere of nitrogen using Schlenk techniques. Anhydrous solvents were obtained via elution through a solvent column drying system. Commercial reagents were distilled prior to their use, except *t*-BuLi. TLC was performed on Merck plates with aluminum backing and silica gel 60 F_{254}. For column chromatography, silica gel 60 (40−63 μm) from Scharlau was used. Phosphazenes **7a**,[42] **7b**,[42] **7d**,[43] and **7g**[43] (precursor of **7f**) used in this study were prepared according to methods described in the literature. The synthesis of spiro[1,2]-oxaphosphetanes **9c**,[23] **9d**,[25] **9e**,[25] **9j**,[25] and **9l**[25] has been reported previously. Compounds **10a** (CAS No. 563−79−1), **10d**/**10p** (CAS No. 769−57−3), **10l** (CAS No. 1003−64−1), and **10m** (CAS No. 778−66−5) are commercial. Compounds **10b**,[44] **10c**,[45] *Z*-**10e**,[19,46] **10d** (=**10p**),[23,47] *E*-**10e**,[19,48] **10j**,[49] **10k**,[50] **10l**,[51] *Z*-**10n**,[48] **10o**,[52] and **11**[19] have been described previously.

X-ray Crystallographic Studies of *cis*-9d, *trans*-9k, and 12a. A suitable crystal of *cis*-**9d**, *trans*-**9k**, and **12a** was covered in Paratone-N (Hampton Research) and mounted onto a MiTeGenmicromount. The crystal was transferred directly to a Nonius Kappa CCD diffractometer with CuKα (λ = 1.54184 Å) for *cis*-**9d**, an Oxford Diffraction Xcalibur Gemini S with MoKα (λ = 0.71073 Å) for *trans*-**9k**, and a Bruker Smart 1000 CCD diffractometer with MoKα (λ = 0.71073 Å) for **12a**. The intensities were measured using the oscillation method. The crystal structures were solved by direct methods for *cis*-**9d** and *trans*-**9k** and Patterson methods for **12a**. The refinement was performed using full-matrix least-squares on F2. All non-H atoms were anisotropically refined. All H atoms were geometrically placed riding on their parent atoms with isotropic displacement parameters set to 1.2 times the Ueq of the atoms to which they are attached (1.5 for methyl groups).

Crystallographic calculations were carried out by the X-ray team, at the University of Oviedo, using the following programs: Collect[53] for data collection and HKL Denzo and Scalepack[54] for cell refinement and data reduction for *cis*-**9d**; Bruker SMART[55] for data collection and cell refinement and Bruker SAINT3[55] for data reduction for **12a**; CrysAlisPro CCD and RES[56] for data collection, cell refinement, and data reduction for *trans*-**9k**; for structure solution SIR-92[57] for *cis*-**9d**, SIR-2004[58] for *trans*-**9k**, DIRDIF-2008[59] for **12a**; XABS2[60] for refined absorption correction; SHELXL-97[61] for structure refinement; WinGX[62] publication routines and enCIFer[63] for preparing material for publication; PLATON[64] for the geometrical calculations; ORTEP-3[65] for windows for molecular graphics. Crystal data and structure

https://dx.doi.org/10.1021/acs.joc.0c01270
J. Org. Chem. XXXX, XXX, XXX−XXX

refinement details for all compounds are outlined in Tables S10−S12. Crystallographic data (excluding structure factors) for the structures reported in this paper have been deposited in The Cambridge Crystallographic Data Centre no. CCDC: 749832 (*cis*-**9d**), CCDC: 749831 (*trans*-**9k**), and CCDC: 846036 (**12a**). These data can be obtained free of charge from the CCDC via http://www.ccdc.cam.ac.uk/products/csd/request/.

Computational Methods. Computations were carried out on the Alhambra supercomputer of the IT and Communications Centre (CSIRC) of the University of Granada using the suite of programs Gaussian 09.[35] Geometry optimizations, vibrational frequency, and natural bond orbital (NBO)[66] calculations were performed using the M06-L-6-31(d) functional.[67] All stationary points located were characterized by performing the harmonic frequency calculations. All minima have zero imaginary frequency, and all transition states have only one imaginary frequency. Intrinsic reaction coordinate (IRC) calculations were performed to establish the connection between ground state, transition state, and products.[68] Single-point energy calculations were carried out using the M06-L functional and basis set 6-311+G(d,p). The SMD[40] solvation model was used in the single-point energy calculations to incorporate solvent effects with toluene or DMSO as the solvents. Thermal corrections to the Gibbs free energies and enthalpies were calculated using the harmonic oscillator approximation at 403.15 K.

***P*-Penthyl-*P*,*P*-(diphenyl)(*N*-methoxycarbonyl)phosphazene (7c).** Compound **7c** has been synthesized using the same procedure reported for **7a**[42] and was isolated by precipitation from diethyl ether in a yield of 85%. White solid. Mp: 99−100 °C. IR (KBr): ν 1625, 1292 cm^{-1}. ^{1}H NMR (300.13 MHz, $CDCl_3$): δ 7.79 (m, 4H, H7), 7.46−7.61 (m, 6H, H8, H9), 3.64 (s, 3H, H11), 2.63 (m, 2H, H1), 1.51 (m, 2H, H2), 1.31 (m, 4H, H3, H4), 0.83 (t, $^3J_{HH}$ = 6.9 Hz, 3H, H5) ppm. ^{13}C{^{1}H} NMR (75.47 MHz, $CDCl_3$): δ 162.7 (d, $^2J_{PC}$ = 1.7 Hz, C10), 132.9 (d, $^2J_{PC}$ = 9.2 Hz, C7), 132.2 (d, $^4J_{PC}$ = 1.9 Hz, C9), 128.4 (d, $^3J_{PC}$ = 12.1 Hz, C8), 125.8 (d, $^1J_{PC}$ = 93.8 Hz, C6), 53.5 (d, $^4J_{PC}$ = 3.7 Hz, C11), 29.7 (d, $^3J_{PC}$ = 13.0 Hz, C3), 28.6 (d, $^2J_{PC}$ = 1.6 Hz, C2), 23.0 (d, $^1J_{PC}$ = 65.2 Hz, C1), 13.8 (C5), 22.4 (C4) ppm. ^{31}P{^{1}H} NMR (121.50 MHz, $CDCl_3$): δ 25.9 ppm. HRMS (ESI/TOF) *m*/*z*: [M + 1] calcd for $C_{19}H_{25}NO_2P$, 330.1623; found, 330.1638.

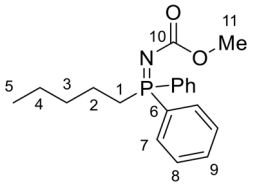

Methyl (Diphenyl(1-phenylethyl)-λ^5-phosphanylidene)-carbamate (7f). Compound **7f** has been synthesized through α-lithiation of **7g**[43] followed by electrophilic quench with methyl iodide using the same procedure reported in the literature for the α-alkylation of phosphazenes.[43] Compound **7f** was isolated by precipitation from diethyl ether in a yield of 66%. White solid. Mp: 135−136 °C. IR (KBr): ν 1625, 1311 cm^{-1}. ^{1}H NMR (300.13 MHz, $CDCl_3$): δ 7.76 (m, 2H, H11$^{\#}$), 7.55 (m, 4H, H7$^{\#}$, H9, H13), 7.48 (m, 2H, H12*), 7.38 (m, 2H, H8*), 7.16 (m, 3H, H4, H5), 6.92 (m, 2H, H3), 4.51 (dq, $^2J_{PH}$ = 15.9 Hz, $^3J_{HH}$ = 7.5 Hz, 1H, H1), 3.61 (s, 3H, H16), 1.61 (dd, $^3J_{PH}$ = 16.9 Hz, $^3J_{HH}$ = 7.5 Hz, 3H, H14) ppm. ^{13}C{^{1}H} NMR (75.47 MHz, $CDCl_3$): δ 162.8 (d, $^2J_{PC}$ = 2.4 Hz, C15), 136.3 (d, $^2J_{PC}$ = 5.6 Hz, C2), 133.3 (d, $^2J_{PC}$ = 8.7 Hz, C11), 133.2 (d, $^2J_{PC}$ = 8.7 Hz, C7), 132.4 (d, $^4J_{PC}$ = 2.8 Hz, C13), 132.2 (d, $^4J_{PC}$ = 2.8 Hz, C9), 128.4 (d, $^3J_{PC}$ = 11.6 Hz, C12), 128.1 (d, $^3J_{PC}$ = 11.6 Hz, C8), 128.1 (d, $^4J_{PC}$ = 2.8 Hz, C4), 127.4 (d, $^5J_{PC}$ = 3.3 Hz, C5), 125.4 (d, $^1J_{PC}$ = 95.8 Hz, C10), 125.3 (d, $^1J_{PC}$ = 94.8 Hz, C6), 52.7 (d, $^4J_{PC}$ = 3.7 Hz, C16), 37.3 (d, $^1J_{PC}$ = 58.7 Hz, C1), 15.6 (d, $^2J_{PC}$ = 1.9 Hz, C14) ppm. ^{31}P{^{1}H} NMR (121.50 MHz, $CDCl_3$): δ 29.94 ppm. HRMS (ESI/TOF) *m*/*z*: [M + 1] calcd for $C_{22}H_{23}NO_2P$, 364.1466; found, 330,1478. *,$^{\#}$ Interchangeables.

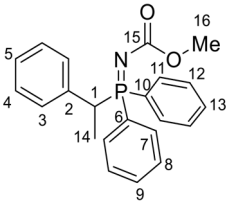

Synthesis. *General Procedure for the Synthesis of Spiro-1,2-oxaphosphetanes **9a−b, f−i, k, m−p**.* To a solution of the appropriate phosphazene **7** (6.64×10^{-4} mol) in THF (10 mL) was added a solution of *t*-BuLi (0.86 mL of a 1.7 M solution in cyclohexane, 1.46×10^{-3} mol) at −35 °C. After 30 min of metalation, the corresponding carbonyl compound was added (0.66×10^{-3} mol). The reaction mixture was stirred at −95 °C for 2.5 h (for the reaction of lithiated **7e**/**7d** with acetophenone/4,4′-bis(dimethylamino)-benzophenone, this time was increased to 5 and 15 h, respectively, and in the latter case, the temperature used was −35 °C) and then quenched with MeOH. The reaction mixture was poured into water and extracted with dichloromethane (2×15 mL). The organic layers were dried over Na_2SO_4 and concentrated *in vacuo*. ^{1}H, ^{1}H{^{31}P}, and ^{31}P{^{1}H} NMR spectra of the crude reaction were always measured in order to determine the stereoselectivity and conversion of the process. The crude mixture was purified by flash column chromatography (eluent: a mixture of ethyl acetate/hexane) or by precipitation from diethyl ether to give **9a−p**.

*3′,3′,4′,4′-Tetramethyl-1-phenyl-1H-spiro[2,1-benzazaphosphole-1,2′-[1,2]oxaphosphetan]-3(2H)-one (**9a**).* Conversion: 92%. Yield after precipitation from diethyl ether: 85%. White solid. Mp: 195−196 °C. IR (KBr): ν 3435, 3140, 1675 cm^{-1}. ^{1}H NMR (300.13 MHz, $CDCl_3$): δ 8.20 (m, 1H, H9), 8.05 (m, 3H, H12, H14), 7.67 (m, 2H, H10, H11), 7.41 (m, 3H, H15, H16), 6.43 (d, $^2J_{PH}$ = 10.5 Hz, 1H, H5), 1.45 (d, $^3J_{PH}$ = 26.8 Hz, 3H, H17), 1.33 (s, 3H, H19), 1.28 (s, 3H, H20), 1.23 (d, $^3J_{PH}$ = 26.8 Hz, 3H, H18) ppm. ^{13}C{^{1}H} NMR (75.47 MHz, $CDCl_3$): δ 168.2 (d, $^2J_{PC}$ = 4.2 Hz, C6), 138.2 (d, $^2J_{PC}$ = 11.7 Hz, C7), 136.8 (d, $^1J_{PC}$ = 147.8 Hz, C8), 135.5 (d, $^1J_{PC}$ = 142.4 Hz, C13), 135.5 (d, $^2J_{PC}$ = 12.0 Hz, C9), 134.7 (d, $^2J_{PC}$ = 12.0 Hz, C14), 132.9 (d, $^4J_{PC}$ = 3.0 Hz, C11), 131.9 (d, $^3J_{PC}$ = 15.6 Hz, C10), 131.1 (d, $^4J_{PC}$ = 3.6 Hz, C16), 128.4 (d, $^3J_{PC}$ = 15.0 Hz, C15), 124.4 (d, $^3J_{PC}$ = 12.0 Hz, C12), 72.1 (d, $^2J_{PC}$ = 16.2 Hz, C4), 64.2 (d, $^1J_{PC}$ = 109.9 Hz, C3), 27.0 (d, $^3J_{PC}$ = 6.6 Hz, C20), 26.0 (d, $^3J_{PC}$ = 6.6 Hz, C19), 21.0 (d, $^2J_{PC}$ = 6.0 Hz, C17, C18) ppm. ^{31}P{^{1}H} NMR (121.50 MHz, $CDCl_3$): δ −63.9 ppm. HRMS (ESI/TOF) *m*/*z*: [M + 1] calcd for $C_{19}H_{23}NO_2P$, 328.1466; found, 328.1469.

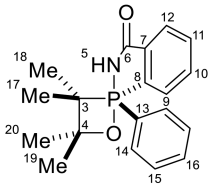

*3′,3′-Dimethyl-1-phenyl-1H-dispiro[2,1-benzazaphosphole-1,2′-[1,2]oxaphosphetane-4′,1″-cyclohexan]-3(2H)-one (**9b**).* Conversion (a = axial, e = equatorial): 93%. Yield after precipitation from diethyl ether 87%. White solid. Mp: 207−208 °C. IR (KBr): ν 3430, 1672 cm^{-1}. ^{1}H NMR (300.13 MHz, $CDCl_3$): δ 8.25 (m, 1H, H9), 7.97−8.12 (m, 3H, H12, H14), 7.58−7.72 (m, 2H, H10, H11), 7.26−7.41 (m, 3H, H15, H16), 6.23 (d, $^2J_{PH}$ = 9.8 Hz, 1H, H5), 1.57−1.95 (m, 5H, H19$_e$, H19′$_e$, H20, H20′, H21$_e$), 1.45 (d, $^3J_{PH}$ = 26.8 Hz, 3H, H17), 1.19 (d, $^3J_{PH}$ = 26.8 Hz, 3H, H18), 1.18−1.38 (m, 3H, H19$_a$, H19′$_a$, H21$_a$) ppm. ^{13}C{^{1}H} NMR (75.47 MHz, $CDCl_3$): δ 168.5 (d, $^2J_{PC}$ = 4.2 Hz, C6), 138.3 (d, $^2J_{PC}$ = 10.8 Hz, C7), 137.5 (d, $^1J_{PC}$ = 147.2 Hz, C8), 135.9 (d, $^1J_{PC}$ = 142.4 Hz, C13), 135.3 (d, $^2J_{PC}$ = 12.0 Hz, C9), 135.0 (d, $^2J_{PC}$ = 12.0 Hz, C14), 132.7 (d, $^4J_{PC}$ = 3.0 Hz, C11), 131.7 (d, $^3J_{PC}$ = 15.0 Hz, C10), 131.0 (d, $^4J_{PC}$ = 3.0 Hz, C16), 128.2 (d, $^3J_{PC}$ = 14.4 Hz, C15), 124.2 (d, $^3J_{PC}$ = 11.4 Hz, C12), 72.8 (d, $^2J_{PC}$ = 16.2 Hz, C4), 64.7 (d, $^1J_{PC}$ = 108.7 Hz, C3), 34.9 (d, $^3J_{PC}$ = 5.4 Hz, C19′), 33.9 (d, $^3J_{PC}$ = 6.6 Hz, C19), 25.4 (C21), 22.7 (C20′), 22.6 (C20), 19.8 (d, $^2J_{PC}$ = 6.0 Hz, C17, C18) ppm. ^{31}P{^{1}H} NMR (121.50 MHz, $CDCl_3$): δ

https://dx.doi.org/10.1021/acs.joc.0c01270
J. Org. Chem. XXXX, XXX, XXX−XXX

−64.7 ppm. HRMS (ESI/TOF) m/z: [M + 1] calcd for $C_{22}H_{27}NO_2P$, 368.1779; found, 368.1791.

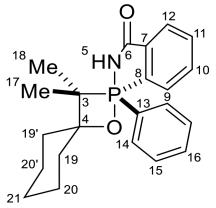

*4′,4′-Bis(4-fluorophenyl)-3′,3′-dimethyl-1-phenyl-1H-spiro[2,1-benzazaphosphole-1,2′-[1,2]oxaphosphetan]-3(2H)-one (**9f**).* Conversion: 93%. Yield after precipitation from diethyl ether: 90%. White solid. Mp: 224−227 °C. IR (KBr): ν 3435, 3155, 1672 cm^{-1}. ^{1}H NMR (500.13 MHz, $CDCl_3$, 25 °C) δ 8.69 (dddd, $^3J_{PH}$ = 12.7 Hz, $^3J_{HH}$ = 7.5 Hz, $^4J_{HH}$ = 1.2 Hz, $^5J_{HH}$ = 0.5 Hz, 1H, H9), 8.01 (dddd, $^3J_{HH}$ = 7.5 Hz, $^4J_{PH}$ = 3.5 Hz, $^4J_{HH}$ = 1.2 Hz, $^5J_{HH}$ = 0.5 Hz, 1H, H12), 7.81 (tdd, H10, $^3J_{HH}$ = 7.5 Hz, $^4J_{PH}$ = 5.2 Hz, $^4J_{HH}$ = 1.2 Hz, 1H, H10), 7.69−7.78 (m, 2H, H11 and H14), 7.57 (ddd, $^3J_{HH}$ = 8.9 Hz, $^4J_{FH}$ = 5.3 Hz, $^4J_{HH}$ = 2.7 Hz, 2H, H20′), 7.31−7.33 (ddd, $^3J_{HH}$ = 8.9 Hz, $^4J_{FH}$ = 5.4 Hz, $^4J_{HH}$ = 2.7 Hz, 2H, H20), 7.20−7.30 (m, 4H, H5, H15, H16), 6.95 (td, $^3J_{HH}$ = $^3J_{FH}$ = 8.9 Hz, $^4J_{HH}$ = 2.7 Hz, 2H, H21′), 6.73 (td, $^3J_{HH}$ = $^3J_{FH}$ = 8.9 Hz, $^4J_{HH}$ = 2.7 Hz, 2H, H21), 1.66 (d, $^3J_{PH}$ = 26.7 Hz, 3H, H17), 1.22 (d, $^3J_{PH}$ = 26.5 Hz, 3H, H18) ppm. ^{13}C{^{1}H} NMR (125.76 MHz, $CDCl_3$, 25 °C) δ 168.1 (d, $^2J_{PC}$ = 6.0 Hz, C6), 161.3 (d, $^1J_{FC}$ = 245.4 Hz, C22), 161.2 (d, $^1J_{FC}$ = 245.7 Hz, C22′), 142.1 (dd, $^3J_{PC}$ = 11.5 Hz, $^4J_{FC}$ = 2.9 Hz, C19′), 140.3 (t, $^3J_{PC}$ = $^4J_{FC}$ = 3.1 Hz, C19), 138.4 (d, $^2J_{PC}$ = 10.8 Hz, C7), 136.9 (d, $^1J_{PC}$ = 140.8 Hz, C8), 135.8 (d, $^1J_{PC}$ = 152.8 Hz, C13), 135.4 (d, $^2J_{PC}$ = 11.3 Hz, C9), 133.1 (d, $^4J_{PC}$ = 2.9 Hz, C11), 132.2 (d $^3J_{PC}$ = 15.6 Hz, C10), 131.8 (d, $^2J_{PC}$ = 11.0 Hz, C14), 130.2 (d, $^4J_{PC}$ = 3.4 Hz, C16), 128.6 (d, $^3J_{FC}$ = 7.9 Hz, C20), 128.0 (d, $^3J_{PC}$ = 14.6 Hz, C15), 127.5 (d, $^3J_{FC}$ = 7.9 Hz, C20′), 124.7 (d, $^3J_{PC}$ = 12.2 Hz, C12), 114.7 (d, $^2J_{FC}$ = 21.4 Hz, C21), 114.1 (d, $^2J_{FC}$ = 21.1 Hz, C21′), 79.1 (d, $^2J_{PC}$ = 13.2 Hz, C4), 68.2 (d, $^1J_{PC}$ = 112.8 Hz, C3), 23.8 (d, $^2J_{PC}$ = 5.0 Hz, C18), 23.7 (d, $^2J_{PC}$ = 4.5 Hz, C17) ppm. ^{31}P{^{1}H} NMR (202.46 MHz, $CDCl_3$, 25 °C) δ −65.4 ppm. ^{19}F{^{1}H} NMR (282.40 MHz, $CDCl_3$, 25 °C) δ −117.4 and −117.1 ppm. HRMS (ESI/TOF) m/z: [M + 1] calcd for $C_{23}H_{25}F_2NO_2P$, 488,1591; found, 488.1589.

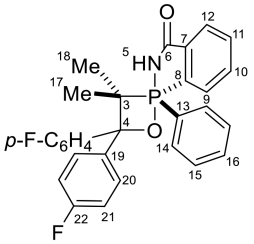

*4′,4′-Bis(4-chlorophenyl)-3′,3′-dimethyl-1-phenyl-1H-spiro[2,1-benzazaphosphole-1,2′-[1,2]oxaphosphetan]-3(2H)-one (**9g**).* Conversion: 95%. Yield after precipitation from diethyl ether: 88%. White solid. Mp: 214−215 °C. IR (KBr): ν 3415, 3151, 1669 cm^{-1}. ^{1}H NMR (500.13 MHz, $CDCl_3$, 25 °C) δ 8.67 (dddd, $^3J_{PH}$ = 12.7 Hz, $^3J_{HH}$ = 7.6 Hz, $^4J_{HH}$ = 1.2 Hz, $^5J_{HH}$ = 0.5 Hz, 1H, H9), 8.00 (dddd, $^3J_{HH}$ = 7.6 Hz, $^4J_{PH}$ = 3.5 Hz, $^4J_{HH}$ = 1.2 Hz, $^5J_{HH}$ = 0.5 Hz, 1H, H12), 7.53 (dd, $^3J_{HH}$ = 8.6 Hz, $^4J_{HH}$ = 2.1 Hz, 2H, H20′), 7.69−7.84 (m, 4H, H10, H11, H14), 7.21−7.37 (m, 8H, H21′, H20, H15, H16, H5), 7.01 (dd, $^3J_{HH}$ = 8.7 Hz, $^4J_{HH}$ = 2.3 Hz, 2H, H21), 1.67 (d, $^3J_{PH}$ = 26.7 Hz, 3H, H17), 1.21 (d, $^3J_{PH}$ = 26.6 Hz, 3H, H18) ppm. ^{13}C{^{1}H} NMR (75.47 MHz, $CDCl_3$): δ 168.1 (d, $^2J_{PC}$ = 6.2 Hz, C6), 144.6 (d, $^3J_{PC}$ = 11.5 Hz, C19′), 142.9 (d, $^3J_{PC}$ = 3.6 Hz, C19), 138.3 (d, $^2J_{PC}$ = 11.0 Hz, C7), 136.8 (d, $^1J_{PC}$ = 141.3 Hz, C8), 135.7 (d, $^1J_{PC}$ = 152.6 Hz, C13), 135.4 (d, $^2J_{PC}$ = 11.3 Hz, C9), 133.2 (d, $^4J_{PC}$ = 3.1 Hz, C11), 132.4 (C22), 132.3 (C22′), 132.3 (d, $^3J_{PC}$ = 15.1 Hz, C10), 131.8 (d, $^2J_{PC}$ = 11.0 Hz, C14), 130.3 (d, $^4J_{PC}$ = 3.4 Hz, C16), 128.3 (C21), 128.1 (C21′), 128.0 (d, $^3J_{PC}$ = 14.6 Hz, C15), 127.43 (C20), 127.3 (C20′), 124.7 (d, $^3J_{PC}$ = 12.5 Hz, C12), 79.1 (d, $^2J_{PC}$ = 13.0 Hz, C4), 68.2 (d, $^1J_{PC}$ = 113.2 Hz, C3), 23.7 (d, $^2J_{PC}$ = 5.3 Hz, C18), 23.7 (d, $^2J_{PC}$ = 5.3 Hz, C17) ppm. ^{31}P{^{1}H} NMR (202.46 MHz, $CDCl_3$, 25 °C) δ −65.4 ppm. HRMS (ESI/TOF) m/z: [M + 1] calcd for $C_{30}H_{29}Cl_2NO_2P$, 536.1313; found, 536.1328.

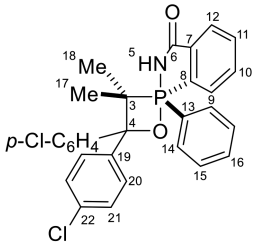

*4′,4′-Bis[3-(trifluoromethyl)phenyl]-3′,3′-dimethyl-1-phenyl-1H-spiro[2,1-benzazaphosphole-1,2′-[1,2]oxaphosphetan]-3(2H)-one (**9h**).* Conversion: 97%. Yield after precipitation from diethyl ether: 89%. White solid. Mp: 214−216 °C. IR (KBr): ν 3473, 1671, 1326, 1166, 1122 cm^{-1}. ^{1}H NMR (300.13 MHz, $CDCl_3$): δ 8.78 (dd, $^3J_{PH}$ = 12.5 Hz, $^3J_{HH}$ 7.5 Hz, 1H, H9), 8.41 (d, $^2J_{PH}$ = 10.6 Hz, 1H, H5), 7.99−8.10 (m, 2H, H12, H20′), 7.80−7.93 (m, 3H, H10, H14), 7.68−7.79 (m, 3H, H11, H22′, H24′), 7.57−7.64 (m, 1H, H24), 7.36−7.50 (m, 2H, H20, H23′), 7.15−7.34 (m, 5H, H15, H16, H22, H23), 1.19 (d, $^3J_{PH}$ 26.2 Hz, 3H, H18), 1.71 (d, $^3J_{PH}$ = 26.8 Hz, 3H, H17) ppm. ^{13}C{^{1}H} NMR (75.47 MHz, $CDCl_3$): δ 168.6 (d, $^2J_{PC}$ = 6.7 Hz, C6), 146.9 (d, $^3J_{PC}$ = 11.3 Hz, C19′), 145.3 (d, $^3J_{PC}$ = 3.5 Hz, C19), 138.4 (d, $^2J_{PC}$ = 11.6 Hz, C7), 136.2 (d, $^1J_{PC}$ = 141.0 Hz, C13), 135.6 (d, $^1J_{PC}$ = 152.4 Hz, C8), 135.4 (d, $^2J_{PC}$ = 11.1 Hz, C9), 133.3 (d, $^4J_{PC}$ = 3.0 Hz, C11), 132.4 (d, $^3J_{PC}$ = 15.3 Hz, C10), 132.0 (d, $^2J_{PC}$ = 11.3 Hz, C14′), 131.8 (d, $^2J_{PC}$ = 11.2 Hz, C14), 130.5 (d, $^4J_{PC}$ = 3.5 Hz, C16), 130.4 (c, $^2J_{FC}$ = 32.1 Hz, C21), 130.2 (c, $^6J_{FC}$ = 1.0 Hz, C24′), 130.0 (c, $^2J_{FC}$ = 32.1 Hz, C21), 129.4 (c, $^6J_{FC}$ = 1.2 Hz, C24), 128.3 (s, C23′), 128.1 (d, $^3J_{PC}$ = 14.8 Hz, C15), 127.7 (s, C23), 124.6 (d, $^3J_{PC}$ = 12.3 Hz, C12), 124.2 (c, $^1J_{FC}$ = 272.3 Hz, C25′), 124.0 (c, $^3J_{FC}$ = 4.0 Hz, C22′), 123.9 (c, $^1J_{FC}$ = 272.6 Hz, C25), 123.5 (c, $^3J_{FC}$ = 3.6 Hz, C20′), 123.4 (c, $^3J_{FC}$ = 3.7 Hz, C22), 123.0 (c, $^3J_{FC}$ = 3.9 Hz, C20), 79.1 (d, $^2J_{PC}$ = 12.7 Hz, C4), 68.4 (d, $^1J_{PC}$ = 113.8 Hz, C3), 23.5 (d, $^2J_{PC}$ = 5.1 Hz, C17, C18) ppm. ^{31}P{^{1}H} NMR δ (121.50 MHz, $CDCl_3$): −65.1 ppm. ^{19}F{^{1}H} NMR (282.4 MHz, $CDCl_3$): δ −62.6, −62.5 ppm. HRMS (ESI/TOF) m/z: [M + 1] calcd for $C_{31}H_{25}F_6NO_2P$, 588.1527; found, 588.1535.

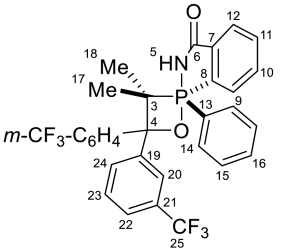

*4′,4′-Bis(4-methylaminophenyl)-3′,3′-dimethyl-1-phenyl-1H-spiro[2,1-benzazaphosphole-1,2′-[1,2]oxaphosphetan]-3(2H)-one (**9i**).* Conversion: 85%. Yield after precipitation from diethyl ether: 73%. White solid. Mp: 125−126 °C, decomp. IR (KBr): ν 3444, 1665 cm^{-1}. ^{1}H NMR (300.13 MHz, $CDCl_3$): δ 8.72 (dddd, $^3J_{PH}$ = 12.5 Hz, $^3J_{HH}$ = 7.4 Hz, $^4J_{HH}$ = 1.1 Hz, $^5J_{HH}$ = 0.5 Hz, 1H, H9), 7.98 (dddd, $^4J_{PH}$ = 3.1 Hz, $^3J_{HH}$ = 7.4 Hz, $^4J_{HH}$ = 1.1 Hz, $^5J_{HH}$ = 0.5 Hz, 1H, H12), 7.73−7.88 (m, 3H, H10, H14), 7.67 (tdd, $^3J_{HH}$ = 7.4 Hz, $^4J_{HH}$ = 1.1 Hz, $^5J_{PH}$ = 2.0 Hz, 1H, H11), 7.47 (dd, $^3J_{HH}$ = 8.7, $^4J_{HH}$ = 2.6 Hz, 2H, H20′), 7.21−7.33 (m, 5H, H15, H16, H20), 6.97 (d, $^2J_{PH}$ = 9.9 Hz, 1H, H5), 6.63 (dd, $^3J_{HH}$ = 8.7, $^4J_{HH}$ = 2.5 Hz, 2H, H21′), 6.46 (dd, $^3J_{HH}$ = 8.9 Hz, $^4J_{HH}$ = 2.5 Hz, 2H, H21), 2.84 (s, 6H, H23), 2.88 (s, 6H, H23′), 1.61 (d, $^3J_{PH}$ = 27.1 Hz, 3H, H17), 1.26 (d, $^3J_{PH}$ = 27.0 Hz, 3H, H18) ppm. ^{13}C{^{1}H} NMR (75.47 MHz, $CDCl_3$): δ 168.1 (d, $^2J_{PC}$ = 5.4 Hz, C6), 148.7 (C22′), 148.6 (C22), 138.3 (d, $^2J_{PC}$ = 10.5 Hz, C7), 137.3 (d, $^1J_{PC}$ = 141.4 Hz, C8), 136.5 (d, $^1J_{PC}$ = 151.3 Hz, C13), 135.7 (d, $^2J_{PC}$ = 11.6 Hz, C9), 135.0 (d, $^3J_{PC}$ = 10.5 Hz, C19′), 133.4 (d, $^3J_{PC}$ = 4.7 Hz, C19), 132.7 (d, $^4J_{PC}$ = 3.0 Hz, C11), 132.2 (d, $^2J_{PC}$ = 11.1 Hz, C14), 131.9 (d, $^3J_{PC}$ = 15.1 Hz, C10), 130.0 (d, $^4J_{PC}$ = 3.1 Hz, C16), 127.9 (d, $^3J_{PC}$ = 14.6 Hz, C15), 127.6 (C20), 126.8 (C20′), 124.4 (d, $^3J_{PC}$ = 12.0 Hz, C12), 111.8 (C21′), 111.5 (C21), 79.7 (d, $^2J_{PC}$ = 13.7 Hz, C4), 68.8 (d, $^1J_{PC}$ = 110.4 Hz, C3), 40.5 (C23), 40.5 (C23′), 24.1 (d, $^2J_{PC}$ = 5.6 Hz,

https://dx.doi.org/10.1021/acs.joc.0c01270
J. Org. Chem. XXXX, XXX, XXX−XXX

C17), 23.9 (d, $^2J_{PC}$ = 5.4 Hz, C18) ppm. $^{31}P\{^1H\}$ NMR (121.50 MHz, $CDCl_3$): δ −64.2 ppm. HRMS (ESI/TOF) m/z: [M + 1] calcd for $C_{33}H_{37}N_3O_2P$, 538.2623; found, 538.2625.

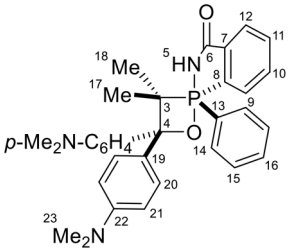

*(1S_P,4′*R*)-4′-[(1*S*,5*R*)-6,6-Dimethyl bicycle[3.1.1]hept-2-en-2-yl]-3′,3′-dimethyl-1-phenyl-1H-spiro[2,1-benzazaphosphole-1,2′-[1,2]-oxaphosphetan]-3(2H)-one (trans-**9k**).*[69] Conversion: 47%. Yield after chromatography (ethyl acetate/hexane 1:1): 39%. Slightly yellow oil. ^1H NMR (300.13 MHz, $CDCl_3$): δ 8.20 (m, 1H, H9), 7.97−8.08 (m, 3H, H14, H12), 7.61−7.72 (m, 2H, H10, H11), 7.38−7.53 (m, 3H, H15, H16), 6.00 (d, $^2J_{PH}$ = 10.2 Hz, 1H, H-5), 5.64 (tq, $^3J_{HH}$ = 3.0 Hz, $^4J_{HH}$ = 1.5 Hz, 1H, H20), 4.25 (dq, $^3J_{PH}$ = 5.5 Hz, J_{HH} = 1.5 Hz, 1H, H4), 2.37 (dt, $^3J_{HH}$ = 5.6 Hz, $^2J_{HH}$ = 8.4 Hz, 1H, H25), 2.33 (m, 2H, H21), 2.17 (t, $^3J_{HH}$ = $^4J_{HH}$ = 5.6 Hz, 1H, H24), 2.12 (m, 1H, H22), 1.39 (d, $^3J_{PH}$ = 27.7 Hz, 3H, H17), 1.28 (s, 3H, H26), 1.20 (d, $^2J_{PH}$ = 8.4 Hz, 1H, H25), 1.19 (d, $^3J_{PH}$ = 26.0 Hz, 3H, H18), 0.93 (s, 3H, H27) ppm. $^{13}C\{^1H\}$ NMR (75.47 MHz, $CDCl_3$): δ 168.6 (d, $^2J_{PC}$ = 3.2 Hz, C6), 147.0 (d, $^3J_{PC}$ = 16.7 Hz, C19), 137.8 (d, $^2J_{PC}$ = 10.7 Hz, C7), 137.1 (d, $^1J_{PC}$ = 154.9 Hz, C8), 135.5 (d, $^2J_{PC}$ = 12.1 Hz, C9), 134.8 (d, $^2J_{PC}$ = 12.1 Hz, C14), 133.4 (d, $^1J_{PC}$ = 137.6 Hz, C13), 132.7 (d, $^4J_{PC}$ = 3.0 Hz, C11), 131.9 (d, $^3J_{PC}$ = 15.8 Hz, C10), 131.4 (d, $^4J_{PC}$ = 3.8 Hz, C16), 128.6 (d, $^3J_{PC}$ = 14.3 Hz, C15), 124.2 (d, $^3J_{PC}$ = 12.8 Hz, C12), 119.8 (C20), 76.4 (d, $^2J_{PC}$ = 17.4 Hz, C4), 66.4 (d, $^1J_{PC}$ = 107.8 Hz, C3), 43.0 (C24), 40.7 (C22), 37.8 (C23), 31.9 (C25), 31.3 (C21), 26.3 (C26), 23.8 (d, $^2J_{PC}$ = 5.3 Hz, C17), 21.9 (C27), 19.4 (d, $^2J_{PC}$ = 6.0 Hz, C18) ppm. $^{31}P\{^1H\}$ NMR (121.50 MHz, $CDCl_3$): δ −63.7 ppm. HRMS (ESI/TOF) m/z: [M + 1] calcd for $C_{26}H_{31}NO_2P$, 420.2092; found, 420.2099.

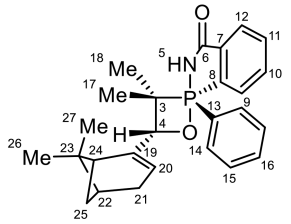

*(1R_P,4′*R*)-4′-[(1*S*,5*R*)-6,6-Dimethyl bicycle[3.1.1]hept-2-en-2-yl]-3′,3′-dimethyl-1-phenyl-1H-spiro[2,1-benzazaphosphole-1,2′-[1,2]-oxaphosphetan]-3(2H)-one (cis-**9k**).* Conversion: 49%. Yield after chromatography (ethyl acetate/hexane 1:1): 43%. Slightly yellow oil. ^1H NMR (300.13 MHz, $CDCl_3$): δ 8.25 (m, 1H, H9), 7.93−8.12 (m, 3H, H14, H12), 7.62−7.78 (m, 2H, H10, H11), 7.33−7.48 (m, 3H, H15, H16), 6.52 (d, $^2J_{PH}$ = 10.7 Hz, 1H, H5), 5.65 (tq, $^3J_{HH}$ = 3.0 Hz, $^4J_{HH}$ = 1.5 Hz, 1H, H20), 4.18 (dq, $^3J_{PH}$ = 7.0 Hz, J_{HH} = 1.5 Hz, 1H, H4), 2.32−2.48 (m, 3H, H25, H21), 2.12 (m, 1H, H22), 1.99 (t, $^3J_{HH}$ = $^4J_{HH}$ = 5.7, 1H, H24), 1.40 (d, $^3J_{PH}$ = 26.4 Hz, 3H, H17), 1.16−1.31 (m, 7H, H18, H25, H26), 0.95 (s, 3H, H27) ppm. $^{13}C\{^1H\}$ NMR (75.47 MHz, $CDCl_3$): δ 168.2 (d, $^2J_{PC}$ = 4.2 Hz, C6), 146.9 (d, $^3J_{PC}$ = 13.2 Hz, C19), 138.8 (d, $^2J_{PC}$ = 10.2 Hz, C7), 135.4 (d, $^1J_{PC}$ = 147.2 Hz, C13), 135.3 (d, $^2J_{PC}$ = 12.0 Hz, C9), 134.9 (d, $^1J_{PC}$ = 143.6 Hz, C8), 134.6 (d, $^2J_{PC}$ = 12.0 Hz, C14), 133.1 (d, $^4J_{PC}$ = 3.0 Hz, C11), 132.0 (d, $^3J_{PC}$ = 15.0 Hz, C10), 131.1 (d, $^4J_{PC}$ = 3.6 Hz, C16), 128.2 (d, $^3J_{PC}$ = 15.0 Hz, C15), 124.7 (d, $^3J_{PC}$ = 11.4 Hz, C12), 119.3 (C20), 77.6 (d, $^2J_{PC}$ = 17.4 Hz, C4), 65.3 (d, $^1J_{PC}$ = 109.9 Hz, C3), 43.1 (C24), 40.8 (C22), 37.7 (C23), 32.0 (C25), 31.3 (C21), 26.3 (C26), 24.3 (d, $^2J_{PC}$ = 5.8 Hz, C17), 21.9 (C27), 19.6 (d, $^2J_{PC}$ = 5.8 Hz, C18) ppm. $^{31}P\{^1H\}$ NMR (121.50 MHz, $CDCl_3$): δ −63.6 ppm. HRMS (ESI/TOF) m/z: [M + 1] calcd for $C_{26}H_{31}NO_2P$, 420.2092; found, 420.2099.

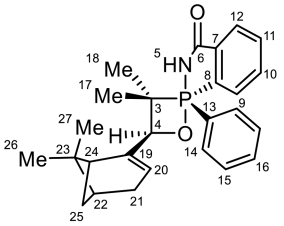

(1R_P,3′*S**)-3′-Methyl-1,4′,4′-triphenyl-1H-spiro[2,1-benzazaphosphole-1,2′-[1,2]oxaphos-phetan]-3(2H)-one (cis-**9m**).*[69] Conversion: 86%. Yield after precipitation from diethyl ether: 80%. White solid. Mp: 192−193 °C. IR (KBr): ν 3425, 3193, 1675 cm^{-1}. ^1H NMR (300.13 MHz, $CDCl_3$): δ 8.40 (m, 1H, H9), 7.85−8.01 (m, 3H, H12, H14), 7.79 (d, $^2J_{PH}$ = 11.0 Hz, 1H, H5), 7.59−7.67 (m, 2H, H10, H11), 7.47−7.55 (m, 2H, H19′), 7.26−7.44 (m, 5H, H15, H16, H19), 7.08−7.25 (m, 6H, H20, H20′, H21, H21′), 4.73 (dq, $^2J_{PH}$ = 24.1 Hz, $^3J_{HH}$ = 8.1 Hz, 1H, H3), 1.51 (dd, $^3J_{PH}$ = 29.2 Hz, $^3J_{HH}$ = 8.1 Hz, 3H, H17) ppm. $^{13}C\{^1H\}$ NMR (75.47 MHz, $CDCl_3$): δ 167.4 (d, $^2J_{PC}$ = 7.2 Hz, C6), 148.4 (d, $^3J_{PC}$ = 7.8 Hz, C18′), 143.3 (d, $^3J_{PC}$ = 6.0 Hz, C18), 138.2 (d, $^2J_{PC}$ = 12.0 Hz, C7), 136.3 (d, $^1J_{PC}$ = 151.3 Hz, C8), 136.1 (d, $^2J_{PC}$ = 12.6 H, C9z), 136.0 (d, $^1J_{PC}$ = 143.0 Hz, C13), 132.9 (d, $^4J_{PC}$ = 2.9 Hz, C11), 132.5 (d, $^2J_{PC}$ = 11.4 Hz, C14), 131.8 (d, $^3J_{PC}$ = 16.2 Hz, C10), 130.5 (d, $^4J_{PC}$ = 3.6 Hz, C16), 128.1 (d, $^3J_{PC}$ = 15.0 Hz, C15), 128.0 (C20), 127.6 (C20′), 126.8 (C19), 126.6 (C21), 126.4 (C21′), 125.8 (C19′), 124.3 (d, $^3J_{PC}$ = 12.6 Hz, C12), 77.5 (d, $^2J_{PC}$ = 15.0 Hz, C4), 63.8 (d, $^1J_{PC}$ = 109.3 Hz, C3), 13.4 (d, $^2J_{PC}$ = 9.6 Hz, C17) ppm. $^{31}P\{^1H\}$ NMR (121.50 MHz, $CDCl_3$): δ −72.4 ppm. HRMS (ESI/TOF) m/z: [M + 1] calcd for $C_{26}H_{31}NO_2P$, 438.1623; found, 438.1635.

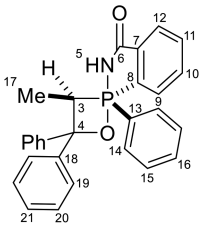

(1R_P,3′*S**,4′*R**)-3′-Buthyl-4′-methyl-1,4′-diphenyl-1H-spiro[2,1-benzazaphosphole-1,2′-[1,2]oxaphosphetan]-3(2H)-one (cis-**9n**).*[69] Conversion: 87%. Yield after precipitation from diethyl ether: 78%. White solid. Mp: 194−195 °C. IR (KBr): ν 3425, 3235, 1678 cm^{-1}. ^1H NMR (300.13 MHz, $CDCl_3$): δ 8.50−8.60 (m, 1H, H9), 8.02−8.10 (m, 1H, H12), 7.79−7.91 (m, 2H, H14), 7.69−7.79 (m, 2H, H10, H11), 0.67 (t, $^3J_{HH}$ = 6.7 Hz, 3H, H20), 7.28−7.46 (m, 4H, H5, H15, H16), 7.15−7.26 (m, 5H, H22, H23, H24), 3.81 (ddd, $^2J_{PH}$ = 23.4 Hz, $^3J_{HH}$ = 10.7 Hz, $^3J_{HH}$ = 3.3 Hz, 1H, H3), 1.77 (s, 3H, H25), 1.47−1.68 (m, 2H, H17), 0.93−1.28 (m, 4H, H18, H19) ppm. $^{13}C\{^1H\}$ NMR (75.47 MHz, $CDCl_3$): δ 167.3 (d, $^2J_{PC}$ = 7.2 Hz, C6), 143.6 (d, $^3J_{PC}$ = 7.9 Hz, C21), 138.3 (d, $^2J_{PC}$ = 11.5 Hz, C7), 137.3 (d, $^1J_{PC}$ = 149.6 Hz, C8), 136.1 (d, $^2J_{PC}$ = 12.1 Hz, C9), 136.0 (d, $^1J_{PC}$ = 144.8 Hz, C13), 133.1 (d, $^4J_{PC}$ = 3.0 Hz, C11), 132.3 (d, $^2J_{PC}$ = 12.1 Hz, C14), 132.0 (d, $^3J_{PC}$ = 15.6 Hz, C10), 130.5 (d, $^4J_{PC}$ = 3.0 Hz, C16), 128.2 (d, $^3J_{PC}$ = 15.0 Hz, C15), 127.7 (C23), 126.8 (C24), 126.5 (C22), 124.5 (d, $^3J_{PC}$ = 12.0 Hz, C12), 74.8 (d, $^2J_{PC}$ = 16.8 Hz, C4), 71.2 (d, $^1J_{PC}$ = 105.7 Hz, C3), 32.0 (d, $^3J_{PC}$ = 6.0 Hz, C25), 31.1 (d, $^3J_{PC}$ = 20.4 Hz, C18), 26.6 (d, $^2J_{PC}$ = 8.4 Hz, C17), 22.4 (d, $^4J_{PC}$ = 1.8 Hz, C19), 13.6 (C20) ppm. $^{31}P\{^1H\}$ NMR (121.50 MHz, $CDCl_3$): δ −75.9 ppm. HRMS (ESI/TOF) m/z: [M + 1] calcd for $C_{26}H_{29}NO_2P$, 418.1936; found, 418.1952.

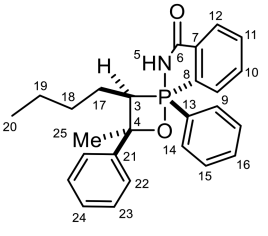

https://dx.doi.org/10.1021/acs.joc.0c01270
J. Org. Chem. XXXX, XXX, XXX−XXX

(1R_P,3′S*)-4′,4′-Bis(4-methoxyphenyl)-3′-methyl-1-phenyl-1H-spiro[2,1-benzazaphosphole-1,2′-[1,2]oxaphos-phetan]-3(2H)-one (cis-**9o**).* Conversion: 83%. Yield after precipitation from diethyl ether: 75%. White solid. Mp: 138−140 °C, decomp. IR (KBr): ν 1683 cm^{-1}. ^{1}H NMR (300.13 MHz, $CDCl_3$): δ 8.39 (m, 1H, H9), 7.96 (m, 1H, H12), 7.84 (m, 2H, H14), 7.59−7.66 (m, 2H, H10, H11), 7.32−7.44 (m, 5H, H15, H16, H19′), 7.08 (dd, $^3J_{HH}$ = 8.8, $^4J_{HH}$ = 2.5 Hz, 2H, H19), 6.95 (d, $^2J_{PH}$ = 11.3 Hz, 1H, H5), 6.81 (dd, $^3J_{HH}$ = 8.6, $^4J_{HH}$ = 2.5 Hz, 2H, H20′), 6.67 (dd, $^3J_{HH}$ = 8.8 Hz, $^4J_{HH}$ = 2.5 Hz, 2H, H20), 4.69 (dq, $^2J_{PH}$ = 24.0 Hz, $^3J_{HH}$ = 7.9 Hz, 1H, H3), 3.76 (s, 3H, H22′), 3.73 (s, 3H, H22), 1.47 (dd, $^3J_{PH}$ = 29.2 Hz, $^3J_{HH}$ = 7.9 Hz, 3H, H17) ppm. ^{13}C{^{1}H} NMR (75.47 MHz, $CDCl_3$): δ 167.9 (d, $^2J_{PC}$ = 7.5 Hz, C6), 158.2 (C21′), 157.9 (C21), 139.9 (d, $^3J_{PC}$ = 8.3 Hz, C18′), 138.1 (d, $^2J_{PC}$ = 10.9 Hz, C7), 136.3 (d, $^3J_{PC}$ = 5.2 Hz, C18), 136.1 (d, $^1J_{PC}$ = 149.8 Hz, C8), 136.1 (d, $^2J_{PC}$ = 12.1 Hz, C9), 135.9 (d, $^1J_{PC}$ = 141.0 Hz, C13), 133.0 (d, $^4J_{PC}$ = 3.1 Hz, C11), 132.3 (d, $^2J_{PC}$ = 11.4 Hz, C14), 131.9 (d, $^3J_{PC}$ 15.3 Hz, C10), 130.5 (d, $^4J_{PC}$ = 3.3 Hz, C16), 128.2 (d, $^3J_{PC}$ = 14.9 Hz, C15), 127.9 (C19), 126.9 (C19′), 124.3 (d, $^3J_{PC}$ = 12.4 Hz, C12), 113.3 (C20′), 112.9 (C20), 79.4 (d, $^2J_{PC}$ = 13.7 Hz, C4), 63.7 (d, $^1J_{PC}$ = 109.0 Hz, C3), 55.1 (C22′), 55.1 (C-22), 13.5 (d, $^2J_{PC}$ = 9.3 Hz, C17) ppm. ^{31}P{^{1}H} NMR (121.50 MHz, $CDCl_3$): δ −72.8 ppm. HRMS (ESI/TOF) m/z: [M + 1] calcd for $C_{30}H_{29}NO_4P$, 418.1834; found, 418.1849.

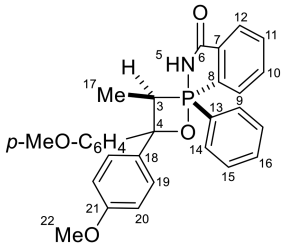

(1R_P,3′R*)-3′,4′,4′-Trimethyl-1,3′-diphenyl-1,2-dihydro-3H-1λ^5-spiro[benzo[c][1,2]aza-phosphole-1,2′-[1,2]oxaphosphetan]-3-one (cis-**9p**).* Conversion: 18%. Yield after two successive chromatographic purifications (ethyl acetate/hexane 2:3): 1%. White solid. Mp: 168−170 °C, decomp. IR (KBr): ν 1668 cm^{-1}. ^{1}H NMR (300.13 MHz, $CDCl_3$): δ 8.33 (m, 2H, H14), 8.13 (m, 1H, H9), 8.02 (m, 1H, H12), 7.65 (m, 1H, H10), 7.62 (m, 1H, H11), 7.5 (m, 1H, H16), 7.47 (m, 2H, H15), 7.25 (m, 5H, H21, H22, H23), 6.19 (d, $^2J_{PH}$ = 11.8 Hz, H5), 1.76 (d, $^3J_{PH}$ = 27.1 Hz, 3H, H18), 1.47 (s, 3H, H20), 1.10 (s, 3H, H19) ppm. ^{13}C{^{1}H} NMR (75.47 MHz, $CDCl_3$): δ 168.8 (d, $^2J_{PC}$ = 4.7 Hz, C6), 141.1 (d, $^2J_{PC}$ = 7.7 Hz, C17), 139.2 (d, $^1J_{PC}$ = 152.3 Hz, C8), 137.8 (d, $^2J_{PC}$ = 10.5 Hz, C7), 134.6 (d, $^2J_{PC}$ = 11.7 Hz, C9), 136.6 (d, $^2J_{PC}$ = 13.0 Hz, C14), 136.4 (d, $^1J_{PC}$ = 134.4 Hz, C13), 132.8 (d, $^4J_{PC}$ = 3.0 Hz, C11), 132.3 (d, $^3J_{PC}$ = 15.6 Hz, C10), 132.0 (d, $^4J_{PC}$ = 3.6 Hz, C16), 129.1 (d, $^3J_{PC}$ = 14.6 Hz, C15), 127.6 (d, $^3J_{PC}$ = 15.1 Hz, C21), 128.9 (C22), 124.7 (d, $^3J_{PC}$ = 12.3 Hz, C12), 127.4 (C23), 75.2 (d, $^1J_{PC}$ = 115.4 Hz, C3), 73.4 (d, $^2J_{PC}$ = 16.1 Hz, C4), 29.7 (d, $^3J_{PC}$ = 2.7 Hz, C19), 26.7 (d, $^3J_{PC}$ = 11.5 Hz, C20), 21.2 (d, $^2J_{PC}$ = 6.9 Hz, C18) ppm. ^{31}P{^{1}H} NMR (121.50 MHz, $CDCl_3$): δ −67.5 ppm. HRMS (ESI/TOF) m/z: [M + 1] calcd for $C_{24}H_{25}NO_2P$, 390.1623; found, 390.1639.

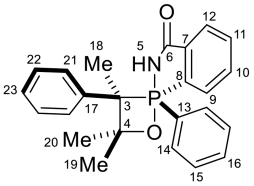

(1R_P,3′S*)-3′,4′,4′-Trimethyl-1,3′-diphenyl-1,2-dihydro-3H-1λ^5-spiro[benzo[c][1,2]aza-phosphole-1,2′-[1,2]oxaphosphetan]-3-one (trans-**9p**).* Identified from a mixture of *cis*-**9p**/*trans*-**9p** in a ratio of 76:24 obtained after purification of a crude reaction mixture through two successive column chromatography separations using ethyl acetate/hexane 2:3 as an eluent. Conversion: 9%. Yield: 0.3%. The amount obtained was too small to achieve the characterization of the mixture. Only the ^{1}H and ^{31}P NMR data are provided. ^{1}H NMR (300.13 MHz, $CDCl_3$): δ 8.08−8.28 (m, 3H, H9, H14), 8.02 (m, 1H, H12), 7.35−7.75 (m, 5H, H11, H10, H15, H16), 7.11−7.21 (m, 5H, H21, H22, H23), 6.07 (d, $^2J_{PH}$ = 11.7 Hz, H5), 1.85 (d, $^3J_{PH}$ = 28.4 Hz, 3H, H18), 1.34 (s, 3H, H20*), 0.95 (s, 3H, H19*) ppm. *Interchangables. ^{31}P{^{1}H} NMR (121.50 MHz, $CDCl_3$): δ −68.73 ppm.

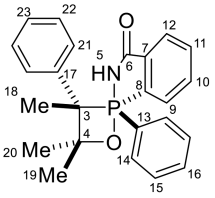

2-(Phenyl(1-phenylethyl)phosphoryl)benzamide (13). Conversion: 35%. Yield after chromatography (ethyl acetate/hexane 2:3): 18%. White solid. Mp: 277−278 °C. IR (KBr): ν 3452, 3130, 1667, 1619, 1166 cm^{-1}. ^{1}H NMR (300.13 MHz, CD_3OD): δ 7.80 (m, 3H, H6, H9), 7.53 (m, 3H, H10, H11), 7.42 (m, 2H, H4, H3), 7.35 (m, 3H, H5, H14), 7.08 (m, 3H, H15, H16), 4.76 (m, 1H, H12), 1.75 (dd, $^3J_{PH}$ = 16.8 Hz, $^3J_{HH}$ = 7.4 Hz, 3H, H17) ppm. ^{13}C{^{1}H} NMR (75.47 MHz, CD_3OD): δ 171.7 (d, $^3J_{PC}$ = 3.6 Hz, C1), 138.5 (d, $^2J_{PC}$ = 8.8 Hz, C2), 138.1 (d, $^2J_{PC}$ = 6.5 Hz, C13), 133.5 (d, $^2J_{PC}$ = 5.8 Hz, C6), 131.8 (d, $^2J_{PC}$ = 9.2 Hz, C9), 131.4 (d, $^1J_{PC}$ = 96.3 Hz, C8), 131.4 (d, $^4J_{PC}$ = 2.8 Hz, C11), 131.1 (d, $^4J_{PC}$ = 2.6 Hz, C4), 130.6 (d, $^1J_{PC}$ = 96.0 Hz, C7), 129.0 (d, $^3J_{PC}$ = 10.4 Hz, C5), 128.7 (d, $^3J_{PC}$ = 5.7 Hz, C14), 127.9 (d, $^3J_{PC}$ = 11.6 Hz, C10), 127.5 (d, $^4J_{PC}$ = 2.5 Hz, C15), 127.2 (d, $^3J_{PC}$ = 9.7 Hz, C3), 126.4 (d, $^5J_{PC}$ = 3.1 Hz, C16), 38.0 (d, $^1J_{PC}$ = 68.4 Hz, C12), 14.4 (d, $^2J_{PC}$ = 3.8 Hz, C17) ppm. ^{31}P{^{1}H} NMR (121.50 MHz, CD_3OD): δ 41.48 ppm. HRMS (ESI/TOF) m/z: [M + 1] calcd for $C_{21}H_{21}NO_2P$, 350.1310; found, 350.1316.

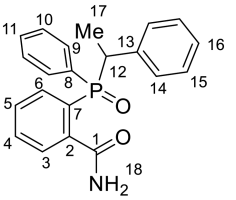

General Procedure for the Synthesis of Spiro-1,2-oxaphosphetanes 12a−d. To a solution of the appropriate phosphazene 7 (6.64×10^{-4} mol) in THF (10 mL) was added a solution of *t*-BuLi (0.86 mL of a 1.7 M solution in cyclohexane, 1.46×10^{-3} mol) at −35 °C. After 30 min of metalation, the corresponding electrophile was added (0.66×10^{-3} mol) at −90 °C, and the mixture was stirred for 2.5 h. Then, the reaction was quenched with methyl trifluoromethanesulfonate (MeOTf, 0.09 mL, 7.97×10^{-4} mol) and stirred for 30 min at −35 °C. The reaction mixture was poured into water and extracted with dichloromethane (2 × 15 mL). The organic layers were dried over Na_2SO_4 and concentrated *in vacuo*, affording a white solid. ^{1}H, ^{1}H{^{31}P}, and ^{31}P{^{1}H} NMR spectra of the crude reaction were always measured in order to determine the conversion of the process. The crude mixture was purified by precipitation from diethyl ether, affording **12a−d**.

*2,3′,3′,4′,4′-Pentamethyl-1-phenyl-1H-spiro[2,1-benzazaphosphole-1,2′-[1,2]oxaphosphetan]-3(2H)-one (**12a**).* Conversion: 95%. Yield after precipitation from diethyl ether: 88%. White solid. Mp: 163−164 °C. IR (KBr): ν 1635 cm^{-1}. ^{1}H NMR (300.13 MHz, $CDCl_3$): δ 8.03−8.14 (m, 2H, H9, H12), 7.62−7.73 (m, 3H, H11, H14), 7.58 (ddt, $^3J_{HH}$ = 7.5 Hz, $^4J_{PH}$ = 4.9 Hz, $^4J_{HH}$ = 1.4 Hz, 1H, H10), 7.28−7.45 (m, 2H, H15, H16), 2.62 (d, $^3J_{PH}$ = 3.0 Hz, 3H, H21), 1.68 (d, $^3J_{PH}$ = 25.2 Hz, 3H, H17), 1.18 (s, 3H, H20), 1.51 (s, 3H, H19), 1.00 (d, $^3J_{PH}$ = 27.7 Hz, 3H, H18) ppm. ^{13}C{^{1}H} NMR (75.47 MHz, $CDCl_3$): δ 166.8 (d, $^2J_{PC}$ = 6.5 Hz, C6), 139.5 (d, $^2J_{PC}$ = 10.2 Hz, C7), 135.8 (d, $^2J_{PC}$ = 11.7 Hz, C9), 134.6 (d, $^2J_{PC}$ = 12.2 Hz, C14), 134.2 (d, $^1J_{PC}$ = 139.4 Hz, C13), 133.0 (d, $^4J_{PC}$ = 3.2 Hz, C11), 132.9 (d, $^1J_{PC}$ = 144.4 Hz, C8), 131.3 (d, $^4J_{PC}$ = 2.9 Hz, C16), 131.2 (d, $^3J_{PC}$ = 15.6 Hz, C10), 128.6 (d, $^3J_{PC}$ = 15.0 Hz, C15), 124.2 (d, $^3J_{PC}$ = 11.4 Hz, C12), 73.7 (d, $^2J_{PC}$ = 16.1 Hz, C4), 66.0 (d, $^1J_{PC}$ = 106.9 Hz, C3), 29.7 (C21), 27.1 (d, $^3J_{PC}$ = 1.7 Hz, C19), 25.7 (d, $^3J_{PC}$ = 11.0 Hz, C20), 21.7 (d, $^2J_{PC}$ = 6.6 Hz, C18), 20.5 (d, $^2J_{PC}$ = 5.2 Hz, C17) ppm. ^{31}P{^{1}H} NMR (121.50 MHz,

https://dx.doi.org/10.1021/acs.joc.0c01270
J. Org. Chem. XXXX, XXX, XXX−XXX

$CDCl_3$): δ −53.4 ppm. HRMS (ESI/TOF) m/z: [M + 1] calcd for $C_{20}H_{25}NO_2P$, 342.1623; found, 342.1641.

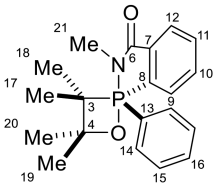

(2′R_P,3′S*)-2,3′-Dimethyl-1,4′,4′-triphenyl-1H-spiro[2,1-benzazaphosphole-1,2′-[1,2]oxaphosphetan]-3(2H)-one (cis-**12b**).* Conversion: 87%. Yield after precipitation from diethyl ether: 80%. White solid. Mp: 163−165 °C. IR (KBr): ν 1665 cm^{-1}. ^1H NMR (300.13 MHz, $CDCl_3$): δ 8.02 (dd, $^4J_{PH}$ = 3.1 Hz, $^3J_{HH}$ = 7.5 Hz, 1H, H12), 7.90 (dd, $^3J_{PH}$ = 13.3 Hz, $^3J_{HH}$ = 7.5 Hz, 1H, H9), 7.64 (m, 2H, H14), 7.50−7.58 (m, 3H, H11, H19), 7.37−7.49 (m, 5H, H15, H16, H20), 7.23−7.36 (m, 4H, H19′, H21, H10), 7.12−7.19 (m, 2H, H20′), 7.01−7.10 (m, 1H, H21′), 4,70 (dq, $^2J_{PH}$ = 19.7 Hz, $^3J_{HH}$ = 8.0 Hz, 1H, H3), 2.64 (d, $^3J_{PH}$ = 2.6 Hz, 3H, H22), 1.64 (d, $^3J_{HH}$ = 8.0 Hz, $^3J_{PH}$ = 28.2 Hz, 3H, H17) ppm. $^{13}C\{^1H\}$ NMR (75.47 MHz, $CDCl_3$): δ 166.1 (d, $^2J_{PC}$ = 8.4 Hz, C6), 147.2 (d, $^3J_{PC}$ = 4.2 Hz, C18′), 143.9 (d, $^3J_{PC}$ = 10.2 Hz, C18), 138.9 (d, $^2J_{PC}$ = 12.0 Hz, C7), 136.4 (d, $^2J_{PC}$ = 12.0 Hz, C9), 133.3 (d, $^1J_{PC}$ = 146.6 Hz, C13), 132.8 (d, $^4J_{PC}$ = 3.0 Hz, C11), 132.7 (d, $^1J_{PC}$ = 144.8 Hz, C8), 132.3 (d, $^2J_{PC}$ = 12.6 Hz, C14), 130.9 (d, $^4J_{PC}$ = 3.6 Hz, C16), 130.7 (d, $^3J_{PC}$ = 15.0 Hz, C10), 128.6 (d, $^3J_{PC}$ = 15.7 Hz, C15), 128.1 (C20), 127.8 (C20′), 126.6 (C19), 126.6 (C21), 126.5 (C21′), 126.2 (C19′), 123.9 (d, $^3J_{PC}$ = 12.0 Hz, C12), 78.2 (d, $^2J_{PC}$ = 15.0 Hz, C4), 63.7 (d, $^1J_{PC}$ = 108.7 Hz, C3), 29.7 (C22), 14.0 (d, $^2J_{PC}$ = 10.0 Hz, C17) ppm. $^{31}P\{^1H\}$ NMR (121.50 MHz, $CDCl_3$): δ −59.8 ppm. HRMS (ESI/TOF) m/z: [M + 1] calcd for $C_{29}H_{27}NO_2P$, 452.1779; found, 452.1793.

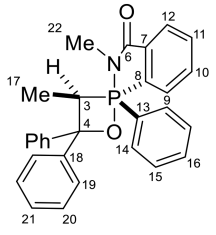

*2,3′,3′-Trimethyl-1,4′,4′-triphenyl-1H-spiro[2,1-benzazaphosphole-1,2′-[1,2]oxa-phosphetan]-3(2H)-one (**12c**).* Conversion: 95%. Yield after precipitation from diethyl ether: 90%. White solid. Mp: 179−180 °C. IR (KBr): ν 1653 cm^{-1}. ^1H NMR (300.13 MHz, $CDCl_3$): δ 8.42 (dd, $^3J_{PH}$ = 12.6 Hz, $^3J_{HH}$ = 7.5 Hz, 1H, H9), 8.07 (ddd, $^4J_{PH}$ = 3.5 Hz, $^3J_{HH}$ = 7.3 Hz, $^4J_{HH}$ = 0.9 Hz, 1H, H12), 7.66−7.71 (m, 2H, H20′), 7.60−7.65 (m, 3H, H10, H14), 7.54−7.59 (m, 1H, H11), 7.29−7.53 (m, 6H, H15, H16, H20, H21′), 7.15−7.27 (m, 3H, H2, H22′), 7.01−7.10 (m, 1H, H22), 2.54 (d, $^3J_{PH}$ = 28.3 Hz, 3H, H23), 1.79 (d, $^3J_{PH}$ = 25.2 Hz, 3H, H17), 1.36 (d, $^3J_{PH}$ = 28.3 Hz, 3H, H18) ppm. $^{13}C\{^1H\}$ NMR (75.47 MHz, $CDCl_3$): δ 166.8 (d, $^2J_{PC}$ = 7.2 Hz, C6), 145.1 (d, $^3J_{PC}$ = 7.6 Hz, C19′), 145.1 (d, $^3J_{PC}$ = 7.2 Hz, C19), 139.0 (d, $^2J_{PC}$ = 11.3 Hz, C7), 136.0 (d, $^2J_{PC}$ = 12.1 Hz, C9), 134.0 (d, $^1J_{PC}$ = 137.3 Hz, C8), 133.1 (d, $^1J_{PC}$ = 155.4 Hz, C13), 133.0 (d, $^4J_{PC}$ = 3.0 Hz, C11), 131.9 (d, $^2J_{PC}$ = 12.2 Hz, C14), 131.1 (d, $^3J_{PC}$ = 15.0 Hz, C10), 130.5 (d, $^4J_{PC}$ = 3.4 Hz, C16), 128.3 (d, $^3J_{PC}$ = 15.5 Hz, C15), 127.9 (C21), 127.5 (C21′), 126.5 (C20 and C20′), 126.3 (C22), 126.2 (C22′), 124.0 (d, $^3J_{PC}$ = 11.6 Hz, C12), 80.4 (d, $^2J_{PC}$ = 13.5 Hz, C4), 68.1 (d, $^1J_{PC}$ = 110.8 Hz, C3), 24.7 (d, $^2J_{PC}$ = 7.0 Hz, C18), 30.5 (C23), 24 (d, $^2J_{PC}$ = 4.7 Hz, C17) ppm. $^{31}P\{^1H\}$ NMR (121.50 MHz, $CDCl_3$): δ −48.9 ppm. HRMS (ESI/TOF) m/z: [M + 1] calcd for $C_{30}H_{29}NO_2P$, 466.1936; found, 466.1952.

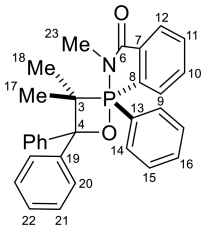

*4′,4′-Bis(4-methoxyphenyl)-2,3′,3′-trimethyl-1-phenyl-1H-spiro-[2,1-benzazaphosphole-1,2′-[1,2]oxaphosphetan]-3(2H)-one (**12d**).* Conversion: 91%. Yield after precipitation from diethyl ether: 87%. White solid. Mp: 183−184 °C. IR (KBr): ν 1685 cm^{-1}. ^1H NMR (300.13 MHz, $CDCl_3$): δ 8.39 (dddd, $^3J_{PH}$ = 13.0 Hz, $^3J_{HH}$ = 7.5 Hz, $^4J_{HH}$ = 1.2 Hz, $^5J_{HH}$ = 0.5 Hz, 1H, H9), 8.06 (dddd, $^4J_{PH}$ = 3.5 Hz, $^3J_{HH}$ = 7.5 Hz, $^4J_{HH}$ = 1.2 Hz, $^5J_{HH}$ = 0.5 Hz, 1H, H12), 7.66 (tdd, $^3J_{HH}$ = 7.4 Hz, $^4J_{HH}$ = 1.2 Hz, $^5J_{PH}$ = 2.0 Hz, 1H, H11), 7.38−7.62 (m, 8H, H16, H20, H20′, H14, H10), 6.89 (dd, $^3J_{HH}$ = 8.9 Hz, $^4J_{HH}$ = 2.5 Hz, 2H, H21), 7.33 (m, 2H, H15), 6.72 (dd, $^3J_{HH}$ = 8.9 Hz, $^4J_{HH}$ = 2.5 Hz, 2H, H21′), 3.83 (s, 3H, H23), 3.71 (s, 3H, H23′), 2.53 (d, $^3J_{PH}$ = 2.9 Hz, 3H, H24), 1.76 (d, $^3J_{PH}$ = 25.4 Hz, 3H, H17), 1.32 (d, $^3J_{PH}$ = 28.3 Hz, 3H, H18) ppm. $^{13}C\{^1H\}$ NMR (75.47 MHz, $CDCl_3$): δ 167 (d, $^2J_{PC}$ = 6.4 Hz, C6), 157.9 (C22′), 157.7 (C22), 139.5 (d, $^2J_{PC}$ = 10.2 Hz, C7), 138.8 (d, $^3J_{PC}$ = 6.1 Hz, C19′), 138.6 (d, $^3J_{PC}$ = 8.8 Hz, C19), 135.9 (d, $^2J_{PC}$ = 12.1 Hz, C9), 134.7 (d, $^1J_{PC}$ = 146.1 Hz, C13), 133 (d, $^4J_{PC}$ = 2.9 Hz, C11), 132.5 (d, $^1J_{PC}$ = 143.2 Hz, C8), 131.8 (d, $^2J_{PC}$ = 12.3 Hz, C14), 131.1 (d, $^3J_{PC}$ = 15.1 Hz, C10), 130.4 (d, $^4J_{PC}$ = 3.5 Hz, C16), 128.3 (d, $^3J_{PC}$ = 15.3 Hz, C15), 127.5 (C20), 127.4 (C20′), 124 (d, $^3J_{PC}$ = 11.6 Hz, C12), 113.2 (C21′), 112.8 (C21), 80.7 (d, $^2J_{PC}$ = 12.9 Hz, C4), 70.4 (d, $^1J_{PC}$ = 107.9 Hz, C3), 55.2 (C23′), 55 (C23), 30.4 (C24), 24.7 (d, $^2J_{PC}$ = 6.9 Hz, C18), 24 (d, $^2J_{PC}$ = 4.6 Hz, C17) ppm. $^{31}P\{^1H\}$ NMR (121.50 MHz, $CDCl_3$): δ −48.7 ppm. HRMS (ESI/TOF) m/z: [M + 1] calcd for $C_{32}H_{33}NO_4P$, 526.2147; found, 526.2156.

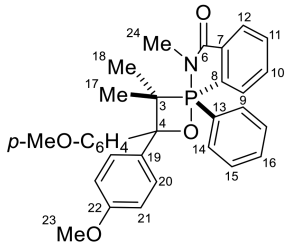

General Procedure for the Synthesis of Olefins 10 and Benzoazaphospholes 11 and 14. A solution of the appropriate 1,2-oxaphosphetane **9**/**12c** (1.3×10^{-4} mol) in DMSO-d_6 (0.5 mL) was heated at 140 °C. After 14 h, 15 mL of water was added, and the reaction mixture was extracted with CH_2Cl_2 (2 × 20 mL). Then the organic layers were dried over Na_2SO_4 and concentrated *in vacuo*. Olefin **10** was extracted with hexane (2 × 5 mL), and the insoluble residue was washed with diethyl ether and identified as the benzoazaphosphol **11**/**14**. All olefins obtained have been described in the literature.

*2,3-Dimethyl-2-butene (**10a**).* Conversion: >97%. Identified from the crude reaction mixture. ^1H NMR (300.13 MHz, DMSO-d_6): δ 1.85 (s, 12H, H2) ppm. ^{13}C NMR (75.47 MHz, $CDCl_3$): δ 124.5 (C1), 20.4 (C2) ppm.

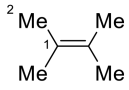

*(1-Methylethylidene)cyclohexane (**10b**).* Conversion: >97%. Colorless oil. Yield: 90%. ^1H NMR (300.13 MHz, $CDCl_3$): δ 2.06 (m, 4H, H2), 1.55 (m, 6H, H6), 1.47 (m, 6H, H3 and H4) ppm.

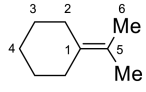

*1,1′-(2-Methylprop-1-ene-1,1-diyl)dibenzene (**10c**).* Conversion: >97%. Colorless oil. Yield: 94%. ^1H NMR (300.13 MHz, $CDCl_3$): δ 7.30 (m, 2H, H5), 7.21 (m, 1H, H7), 7.16 (m, 2H, H6), 1.83 (s, 3H,

https://dx.doi.org/10.1021/acs.joc.0c01270
J. Org. Chem. XXXX, XXX, XXX−XXX

H3) ppm. ^{13}C NMR (75.47 MHz, $CDCl_3$): δ 143.3 (C4), 137.1 (C1), 131.0 (C2), 129.8 (C5), 127.8 (C6), 126.0 (C7), 24.4 (C3) ppm.

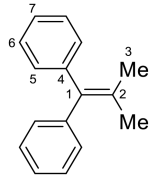

*(1,2-Dimethyl-1-propen-1-yl)-benzene (**10d**).* Conversion: >97%. Colorless oil. Yield: 92%. ^{1}H NMR (300.13 MHz, $CDCl_3$): δ 7.29 (m, 2H, H7), 7.17 (m, 1H, H8), 7.09 (m, 2H, H6), 1.90 (s, 3H, H9), 1.76 (s, 3H, H4), 1.53 (s, 3H, H1) ppm.

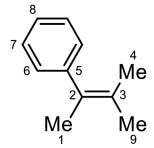

*(Z)-(3-Methylhept-2-en-2-yl)benzene (Z-**10e**).* Conversion: >97%. Colorless oil. Yield: 95%. ^{1}H NMR (300.13 MHz, $CDCl_3$): δ 7.30 (m, 2H, H10), 7.19 (m, 1H, H11), 7.07 (d, $^3J_{HH}$ = 7.5 Hz, 2H, H9), 2.00 (t, $^3J_{HH}$ = 7.5 Hz, 2H, H4), 1.95 (s, 3H, H12), 1.74 (s, 3H, H1), 1.10−1.35 (m, 4H, H5, H6), 0.80 (t, $^3J_{HH}$ = 7.4 Hz, 3H, H7) ppm.

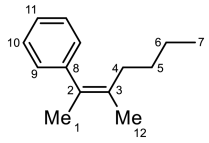

*(E)-(3-Methylhept-2-en-2-yl)benzene (E-**10e**).* Conversion: >97%. Colorless oil. Yield: 96%. ^{1}H NMR (300.13 MHz, $CDCl_3$): δ 7.32 (m, 2H, H10), 7.19 (m, 1H, H11), 7.12 (d, $^3J_{HH}$ = 7.7 Hz, 2H, H9), 2.19 (t, $^3J_{HH}$ = 7.5 Hz, 2H, H4), 1.58 (s, 3H, H1), 1.98 (s, 3H, H12), 1.45 (m, 4H, H5, H6), 0.98 (t, $^3J_{HH}$ = 7.2 Hz, 3H, H7) ppm.

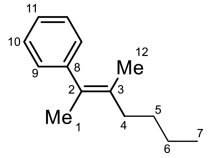

*1-Methoxy-4-(2-dimethyl-1-propen-1-yl)-benzene (**10j**).* Conversion: >97%. Colorless oil. Yield: 95%. ^{1}H NMR (300.13 MHz, $CDCl_3$): δ 7.19 (d, $^3J_{HH}$ = 8.9 Hz, 2H, H6), 6.88 (d, $^3J_{HH}$ = 8.9 Hz, 2H, H7), 6.25 (s, 1H, H1), 3.83 (s, 3H, H9), 1.92 (s, 3H, H3), 1.88 (s, 3H, H4) ppm.

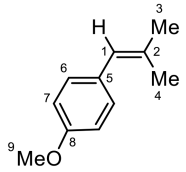

*(1R,5S)-6,6-Dimethyl-2-(2-methylprop-1-enyl)bicyclo[3.1.1]hept-2-ene (Dimethylnopadiene, **10k**).* Conversion: >97%. Colorless oil. Yield: 95%. ^{1}H NMR (300.13 MHz, $CDCl_3$): δ 5.56 (m, 1H, H8), 5.38 (m, 1H, H3), 2.39 (dt, $^4J_{HH}$ = 5.6 Hz, $^2J_{HH}$ = 8.5 Hz, 1H, H7), 2.35 (m, 2H, H4), 2.21 (td, $^3J_{HH}$ = $^4J_{HH}$ = 5.6 Hz, $^4J_{HH}$ = 1.6 Hz, 1H, H1), 2.10 (m, 1H, H5), 1.79 (bs, 3H, H10 or H11), 1.78 (bs, 3H, H10 or H11), 1.30 (s, 3H, H12 or H13), 1.22 (d, 1H, $^3J_{HH}$ = 8.5 Hz, H7), 0.90 (s, 3H, H12 or H13) ppm. ^{13}C NMR (75.47 MHz, $CDCl_3$): δ 145.5 (C, C2), 132.7 (C, C9), 126.1 (CH, C8), 120.4 (CH, C3), 46.7 (CH, C1), 40.5 (CH, C5), 37.7 (C, C6), 31.7 (CH_2, C4), 31.5 (CH_2, C7), 26.7 (CH_3, C10 or C11), 26.3 (CH_3, C12 or C13), 21.1 (CH_3, C12 or C13), 19.9 (CH_3, C10 or C11) ppm.

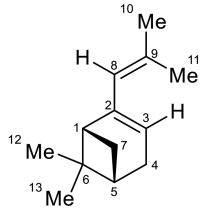

*Ethylidenecyclohexane (**10l**).* Conversion: >97%. Colorless oil. Yield: 92%. ^{1}H NMR (300.13 MHz, $CDCl_3$): δ 5.06 (q, $^3J_{HH}$ = 6.7 Hz, 1H, H5), 2.06 (m, 2H, H2), 2.00 (m, 2H, H2), 1.51 (d, $^3J_{HH}$ = 6.7 Hz, 3H, H6), 1.47 (m, 6H, H3, H4) ppm.

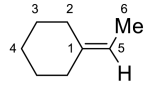

*1,1′-Prop-1-ene-1,1-diyldibenzene (**10m**).* Conversion: >97%. Colorless oil. Yield: 94%. ^{1}H NMR (300.13 MHz, $CDCl_3$): δ 7.22−7.38 (m, 4H, H6), 7.05−7.21 (m, 6H, H5, H7), 6.21 (q, $^3J_{HH}$ = 7.0 Hz, 1H, H2), 1.69 (d, $^3J_{HH}$ = 7.0 Hz, 3H, H3) ppm.

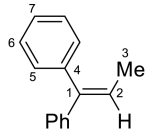

*(Z)-Hept-2-en-2-ylbenzene (**10n**).* Conversion: >97%. Colorless oil. Yield: 94%. ^{1}H NMR (300.13 MHz, $CDCl_3$): δ 7.28 (m, 2H, H10), 7.21 (m, 1H, H11), 7.12 (m, 2H, H9), 5.47 (t, $^3J_{HH}$ = 6.9 Hz, 3H, H3), 2.51 (m, 2H, H4), 2.03 (s, 3H, H1), 1.07−1.37 (m, 4H, H5, H6), 0.83 (t, $^3J_{HH}$ = 7.2 Hz, 3H, H7) ppm.

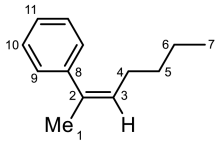

*1,1′-Prop-1-ene-1,1-diylbis(4-methoxybenzene) (**10o**).* Conversion: >97%. Colorless oil. Yield: 94%. ^{1}H NMR (300.13 MHz, $CDCl_3$): δ 6.81 (dd, $^3J_{HH}$ = 8.8 Hz, $^4J_{HH}$ = 2.6 Hz, 2H, H5′), 7.12 (dd, $^3J_{HH}$ = 8.8 Hz, $^4J_{HH}$ = 2.6 Hz, 2H, H5), 6.92 (dd, $^3J_{HH}$ = 8.8 Hz, $^4J_{HH}$ = 2.6 Hz, 2H, H6′), 6.81 (dd, $^3J_{HH}$ = 8.8 Hz, $^4J_{HH}$ = 2.6 Hz, 2H, H6), 6.04 (q, $^3J_{HH}$ = 7.0 Hz, 1H, H2), 3.86 (s, 3H, H8′), 3.81 (s, 3H, H8), 1.77 (d, $^3J_{HH}$ = 7.0 Hz, 3H, H3) ppm.

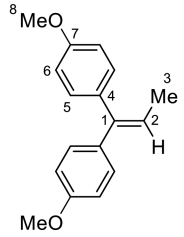

*(S)-1-Phenyl-2-hydrobenzo[c][1,2]azaphosphol-3-one 1-oxide, (S)-**11**.* The byproduct obtained from the olefination of **9k**. The R_P and S_P isomers have been previously characterized.[23] The conditions used for chiral HPLC separation of the enantiomers were as follows: Daicel Chiralcel OD−H-H column, hexane/*i*-PrOH = 7:3, flow rate = 0.5 mL/min, t_R = 8.8 min (R_P), t_R = 14.6 min (S_P).

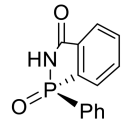

(*S*)-**11**

*2-Methyl-1-phenyl-2-hydrobenzo[c][1,2]azaphosphol-3-one 1-oxide (**14**).* The byproduct obtained in the olefination of oxaphosphetane **12c**. Yield after precipitation from hexane: 99%. Slightly yellow oil. IR (KBr): ν 1703, 1237 cm^{-1}. ^{1}H NMR (300.13 MHz, $CDCl_3$): δ 8.11 (m, 1H, H5), 7.66−7.82 (m, 5H, H6, H7, H8,

https://dx.doi.org/10.1021/acs.joc.0c01270
J. Org. Chem. XXXX, XXX, XXX−XXX

H11), 7.64 (m, 1H, H13), 7.52 (m, 2H, H12), 3.02 (d, $^{3}J_{PH}$ 7.3 Hz, 3H, H14) ppm. $^{13}C\{^{1}H\}$ NMR (75.47 MHz, $CDCl_3$): δ 166.3 (d, $^{2}J_{PC}$ = 22.2 Hz, C3), 135.2 (d, $^{2}J_{PC}$ = 8.6 Hz, C4), 133.6 (d, $^{3}J_{PC}$ = 13.2 Hz, C7), 133.4 (d, $^{4}J_{PC}$ = 2.4 Hz, C6), 133.4 (d, $^{4}J_{PC}$ = 3.1 Hz, C13), 132.2 (d, $^{2}J_{PC}$ = 11.6 Hz, C11), 131.9 (d, $^{1}J_{PC}$ = 118.3 Hz, C9), 129.2 (d, $^{3}J_{PC}$ = 14.0 Hz, C12), 127.9 (d, $^{2}J_{PC}$ = 10.2 Hz, C8), 126.6 (d, $^{1}J_{PC}$ = 129.8 Hz, C10), 124.9 (d, $^{3}J_{PC}$ = 10.3 Hz, C5), 24.4 (d, $^{3}J_{PC}$ = 3.8 Hz, C14) ppm. $^{31}P\{^{1}H\}$ NMR (121.50 MHz, $CDCl_3$): δ 26.92 ppm. HRMS (ESI/TOF) *m/z*: [M + 1] calcd for $C_{14}H_{13}NO_2P$, 258.0684; found, 258.0675.

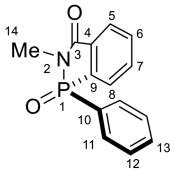

General Procedure for the Determination of Rate Constants of Olefination. The kinetics of the decomposition reaction was monitored by ^{31}P NMR. Samples were prepared by dissolving 10−40 mg of the appropriate spiro-1,2-oxaphosphetane **9**/**12c** in 0.40−0.45 mL of DMSO-d_6 and heated to 70−160 °C. Inverse-gated NMR spectra (pulse width of 15°, relaxation delay of 7 s) were acquired at specific time intervals (see tables in the Supporting Information). Integration of the spectra afforded the relative concentration of **9**, **11**, and **14**.

■ ASSOCIATED CONTENT

Supporting Information

The Supporting Information is available free of charge at https://pubs.acs.org/doi/10.1021/acs.joc.0c01270.

Experimental and computational details, characterization data of starting phosphazenes **7c** and **7f** and known compounds **10** and **11**, rate constants measured, determination of ρ for compounds **9c,f,g,h**, Cartesian coordinates and energies of the stationary points located, NBO charges of selected atoms and groups of atoms, and crystallographic data for *cis*-**9d**, *trans*-**9k**, and **12a** (PDF)
NMR spectra (PDF)
Crystal structure (CIF)

■ AUTHOR INFORMATION

Corresponding Author

Fernando López Ortiz − *Área de Química Orgánica, Centro de Investigación CIAIMBITAL, Universidad de Almería, 04120, Spain;* orcid.org/0000-0003-1786-0157;
Phone: +34950015478; Email: flortiz@ual.es

Authors

Jesús García López − *Área de Química Orgánica, Centro de Investigación CIAIMBITAL, Universidad de Almería, 04120, Spain*

Pablo M. Sansores Peraza − *Área de Química Orgánica, Centro de Investigación CIAIMBITAL, Universidad de Almería, 04120, Spain*

María José Iglesias − *Área de Química Orgánica, Centro de Investigación CIAIMBITAL, Universidad de Almería, 04120, Spain*

Laura Roces − *Departamento de Química Física y Analítica, Universidad de Oviedo-CINN, 33006 Oviedo, Spain; Servicios Científico Técnicos, Universidad de Oviedo, 33006 Oviedo, Spain*

Santiago García-Granda − *Departamento de Química Física y Analítica, Universidad de Oviedo-CINN, 33006 Oviedo, Spain*

Complete contact information is available at: https://pubs.acs.org/10.1021/acs.joc.0c01270

Notes

The authors declare no competing financial interest.

■ ACKNOWLEDGMENTS

Financial support by the Ministerio de Ciencia e Innovación and FEDER program (projects CTQ2008-117BQU, MAT2006-01997, MAT2010-15094, PTA-2009-2346-I, and CSD2006-015, Consolider Ingenio 2010, "Factoría de Crystalización") is gratefully acknowledged.

■ REFERENCES

(1) Staudinger, H.; Meyer, J. Ueber neue organische Phosphorverbindungen III. Phosphinmethylenderivate und Phosphinimine. *Helv. Chim. Acta* **1919**, *2*, 635−646.

(2) Wittig, G.; Geissler, G. Zur Reaktionsweise des Pentaphenylphosphors und einiger Derivate. *Liebigs Ann. Chem.* **1953**, *580*, 44−57.

(3) (a) Kolodiazhnyi, O. I. *Phosphorus Ylides: Chemistry and Applications in Organic Chemistry*; Wiley-VCH: New York, 1999. (b) Soto, A. P.; García-Álvarez, J. Phosphorus Ylides and Related Compounds. In *Organophosphorus Chemistry: From Molecules to Applications*; Iaroshenko, V., Ed.; Wiley-VCH: Weinheim, 2019; pp 113−162.

(4) For recent reviews, see: (a) Rocha, D. H. A.; Pinto, D. C. G. A.; Silva, A. M. S. Applications of the Wittig Reaction on the Synthesis of Natural and Natural- Analogue Heterocyclic Compounds. *Eur. J. Org. Chem.* **2018**, *2018*, 2443−2457. (b) Karanam, P.; Reddy, G. M.; Lin, W. Strategic Exploitation of the Wittig Reaction: Facile Synthesis of Heteroaromatics and Multifunctional Olefins. *Synlett* **2018**, *29*, 2608−2622. (c) Vik, A.; Hansen, T. V. Synthetic Manipulations of Polyunsaturated Fatty Acids as a Convenient Strategy for the Synthesis of Bioactive Compounds. *Org. Biomol. Chem.* **2018**, *16*, 9319−9333. (d) Longwitz, L.; Werner, T. Recent Advances in Catalytic Wittig- type Reactions Based on P(III) /P(V) Redox Cycling. *Pure Appl. Chem.* **2019**, *91*, 95−102. (e) Heravi, M. M.; Ghanbarian, M.; Zadsirjan, V.; Alimadadi-Jani, B. Recent Advances in the Applications of Wittig Reaction in the Total Synthesis of Natural Products Containing Lactone, Pyrone, and Lactam as a Scaffold. *Monatsh. Chem.* **2019**, *150*, 1365−1407. (f) Eschliman, K.; Bossmann, S. H. Synthesis of Isothiocyanates: An Update. *Synthesis* **2019**, *51*, 1746−1752. (g) Zhang, K.; Lu, L.-Q.; Xiao, W.-J. Recent Advances in the Catalytic Asymmetric Alkylation of Stabilized Phosphorous Ylides. *Chem. Commun.* **2019**, *55*, 8716−8721.

(5) Byrne, P. A.; Gilheany, D. G. The Modern Interpretation of the Wittig Reaction Mechanism. *Chem. Soc. Rev.* **2013**, *42*, 6670−6696.

(6) (a) Schlosser, M.; Schaub, B. Cis Selectivity of Salt-Free Wittig Reactions: a "Leeward Approach" of the Aldehyde at the Origin? *J. Am. Chem. Soc.* **1982**, *104*, 5821−5823. (b) Vedejs, E.; Marth, C. F. Mechanism of the Wittig Reaction: the Role of Substituents at Phosphorus. *J. Am. Chem. Soc.* **1988**, *110*, 3948−3958. (c) Vedejs, E.; Fleck, T. J. Kinetic (not Equilibrium) Factors are Dominant in Wittig Reactions of Conjugated Ylides. *J. Am. Chem. Soc.* **1989**, *111*, 5861−5871. (d) Robiette, R.; Richardson, J.; Aggarwal, V. K.; Harvey, J. N. On the Origin of High E Selectivity in the Wittig Reaction of Stabilized Ylides: Importance of Dipole−Dipole Interactions. *J. Am. Chem. Soc.* **2005**, *127*, 13468−13469.

(7) (a) Vedejs, E.; Peterson, M. J. Stereochemistry and Mechanism in the Wittig Reaction. *Top. Stereochem.* **1994**, *21*, 1−157. (b) Vedejs, E.; Peterson, M. J. The Wittig Reaction: Stereoselectivity and a History of Mechanistic Ideas (1953−1995). *Adv. Carbanion Chem.* **1996**, *2*, 1−85.

(8) Stępień, M. Anomalous Stereoselectivity in the Wittig Reaction: The Role of Steric Interactions. *J. Org. Chem.* **2013**, *78*, 9512−9516.

(9) Robiette, R.; Richardson, J.; Aggarwal, V. K.; Harvey, J. N. Reactivity and Selectivity in the Wittig Reaction: A Computational Study. *J. Am. Chem. Soc.* **2006**, *128*, 2394−2409.

(10) (a) Reitz, A. B.; Mutter, M. S.; Maryanoff, B. E. Observation of Cis and Trans Oxaphosphetanes in the Wittig Reaction by High-Field Phosphorus-31 NMR Spectroscopy. *J. Am. Chem. Soc.* **1984**, *106*, 1873−1875. (b) Maryanoff, B. E.; Reitz, A. B.; Mutter, M. S.; Inners, R.

R.; Almond, H. R., Jr. Detailed Rate Studies on the Wittig Reaction of Nonstabilized Phosphorus Ylides via Phosphorus-31, Proton, Carbon-13 NMR Spectroscopy. Insight into Kinetic vs. Thermodynamic Control of Stereochemistry. *J. Am. Chem. Soc.* **1985**, *107*, 1068−1070. (c) Maryanoff, B. E.; Reitz, A. B.; Mutter, M. S.; Whittle, R. R.; Olofson, R. A. Stereochemistry and Mechanism of the Wittig Reaction. Diasteromeric Reaction Intermediates and Analysis of the Reaction Course. *J. Am. Chem. Soc.* **1986**, *108*, 7664−7678.

(11) For recent examples, see: (a) Byrne, P. A.; Muldoon, J.; Ortin, Y.; Müller-Bunz, H.; Gilheany, D. G. Investigations on the Operation of Stereochemical Drift in the Wittig Reaction by NMR and Variable-Temperature NMR Spectroscopy of Oxaphosphetane Intermediates and Their Quench Products. *Eur. J. Org. Chem.* **2014**, *2014*, 86−98. (b) Uchiyama, Y.; Ohtsuki, T.; Murakami, R.; Shibata, M.; Sugimoto, J. (*E*)-Selective Wittig Reactions between a Nonstabilized Phosphonium Ylide Bearing a Phosphastibatriptycene Skeleton and Benzaldehydes. *Eur. J. Org. Chem.* **2017**, *2017*, 159−174. (c) Uchiyama, Y.; Kuniya, S.; Watanabe, R.; Ohtsuki, T. Heteroatom Effects toward Isomerization of Intermediates in Wittig Reactions of Non-Stabilized Phosphonium Ylides Bearing a Phosphaheteratriptycene Skeleton with Benzaldehyde. *Heteroat. Chem.* **2018**, *29*, e21473. (d) Uchiyama, Y.; Kuniya, S.; Watanabe, R.; Ohtsuki, T. Observation of Intermediates in Wittig Reactions of Non- Stabilized Phosphonium Ylides Bearing a Phosphaheteratriptycene Skeleton Containing Group 15 Elements with Benzaldehyde. *Phosphorus, Sulfur Silicon Relat. Elem.* **2019**, *194*, 281−284.

(12) Vedejs, E.; Snoble, K. A. J. Direct Observation of Oxaphosphetanes from Typical Wittig Reactions. *J. Am. Chem. Soc.* **1973**, *95*, 5778−5780.

(13) (a) Vedejs, E.; Meier, G. P.; Snoble, K. A. J. Low-Temperature Characterization of the Intermediates in the Wittig Reaction. *J. Am. Chem. Soc.* **1981**, *103*, 2823−2831. (b) Vedejs, E.; Marth, C. F. Mechanism of Wittig Reaction: Evidence against Betaine Intermediates. *J. Am. Chem. Soc.* **1990**, *112*, 3905−3909. (c) Vedejs, E.; Marth, C. F.; Ruggeri, R. Substituent Effects and the Wittig Mechanism: the Case of Stereospecific Oxaphosphetane Decomposition. *J. Am. Chem. Soc.* **1988**, *110*, 3940−3948.

(14) (a) López-Ortiz, F.; López, J.; Manzaneda, R.; Álvarez, I. Isolable 1,2-Oxaphosphetanes. From Curiosities to Starting Materials for the Synthesis of Olefins. *Mini-Rev. Org. Chem.* **2004**, *1*, 65−70. (b) Kolodiazhna, A. O.; Kolodiazhnyi, O. I. Synthesis, Properties and Stereochemistry of 2- Halo- 1, 2λ^5- oxaphosphetanes. *Molecules* **2016**, *21*, 1371.

(15) Birum, G. H.; Matthews, C. N. Reactions of Triphenyl-2,2-bis(trifluoromethyl)vinyl-idenephosphorane, Synthesized from a Cyclic Ylide-Ketone Adduct. *J. Org. Chem.* **1967**, *32*, 3554−3559.

(16) Ul-Haque, M.; Caughlan, C. N.; Ramirez, F.; Pilot, J. F.; Smith, C. P. Crystal and Molecular Structure of a Four-Membered Cyclic Oxyphosphorane with Pentavalent Phosphorus, $PO_2(C_6H_5)_2(CF_3)_4$-C_3H_2. *J. Am. Chem. Soc.* **1971**, *93*, 5229−5235.

(17) Appel, M.; Blaurock, S.; Berger, S. A Wittig Reaction with 2-Furyl Substituents at the Phosphorus Atom: Improved (Z) Selectivity and Isolation of a Stable Oxaphosphetane Intermediate. *Eur. J. Org. Chem.* **2002**, *2002*, 1143−1148.

(18) Kawashima, T.; Kato, K.; Okazaki, R. A Novel Synthetic Route to Isolable Pentacoordinate 1,2-Oxaphosphetanes and Mechanism of their Thermolysis, the Second Step of the Wittig Reaction. *J. Am. Chem. Soc.* **1992**, *114*, 4008−4010.

(19) García-López, J.; Peralta-Pérez, E.; Forcén-Acebal, A.; García-Granda, S.; López-Ortiz, F. Dilithiated Phosphazenes: Scaffolds for the Synthesis of Olefins through a New Class of Bicyclic 1,2-Oxaphosphetanes. *Chem. Commun.* **2003**, 856−857.

(20) Dellus, N.; Kato, T.; Bagán, X.; Saffron-Merceron, N.; Branchadell, V.; Baceiredo, A. An Isolable Mixed P,S-Bis(ylide) as an Asymmetric Carbon Atom Source. *Angew. Chem., Int. Ed.* **2010**, *49*, 6798−6801.

(21) (a) Granoth, I.; Martin, J. C. Hydroxyphosphoranes and Phosphoranoxide Anions - Synthesis, Reactivity, and Acidity of Pentacoordinate Phosphorus acids. *J. Am. Chem. Soc.* **1979**, *101*, 4618−4622. (b) Perozzi, E. F.; Michalak, R. S.; Figuly, G. D.; Stevenson, W. H., III; Dess, D. B.; Ross, M. R.; Martin, J. C. Directed Dilithiation of Hexafluorocumyl Alcohol - Formation of a Reagent for the Facile Introduction of a Stabilizing Bidentate Ligand in Compounds of Hypervalent Sulfur (10-S-4), Phosphorus (10-P-5), Silicon (10-Si-5), and Iodine (10-I-3). *J. Org. Chem.* **1981**, *46*, 1049−1053.

(22) (a) Kojima, S.; Sugino, M.; Matsukawa, S.; Nakamoto, M.; Akiba, K.-Y. First Isolation and Characterization of an Anti-Apicophilic Spirophosphorane Bearing an Oxaphosphetane Ring: A Model for the Possible Reactive Intermediate in the Wittig Reaction. *J. Am. Chem. Soc.* **2002**, *124*, 7674−7675. (b) Uchiyama, Y.; Kano, N.; Kawashima, T. Syntheses, Structures, and Thermolyses of Pentacoordinate 1,2-Oxastibetanes: Potential Intermediates in the Reactions of Stibonium Ylides with Carbonyl Compounds. *J. Org. Chem.* **2006**, *71*, 659−670.

(23) García López, J.; Morán Ramallal, A.; González, J.; Roces, L.; García-Granda, S.; Iglesias, M. J.; Oña-Burgos, P.; López Ortiz, F. Mechanisms of Stereomutation and Thermolysis of *Spiro*-1,2-oxaphosphetanes: New Insights into the Second Step of the Wittig Reaction. *J. Am. Chem. Soc.* **2012**, *134*, 19504−19507.

(24) Kawashima, T.; Kato, K.; Okazaki, R. Synthesis, Structure, and Thermolysis of a 3-Methoxycarbonyl-1, 2 λ^5-oxaphosphetane. *Angew. Chem., Int. Ed. Engl.* **1993**, *32*, 869−870.

(25) García-López, J.; Fernández, I.; Serrano-Ruiz, M.; López-Ortiz, F. C_{α},C_{ortho}-Dimetalated Phosphazene Complexes. *Chem. Commun.* **2007**, 4674−4676.

(26) For recent computational work, see: (a) Jarwal, N.; Thankachan, P. P. Theoretical Study of the Wittig Reaction of Cyclic Ketones with Phosphorus Ylide. *J. Mol. Model.* **2015**, *21*, 87. (b) Ayub, K.; Ludwig, R. Gas Hydrates Model for the Mechanistic Investigation of the Wittig Reaction "on Water". *RSC Adv.* **2016**, *6*, 23448−23458. (c) Jarwal, N.; Meena, J. S.; Thankachan, P. P. The *E*/*Z* Selectivity in Gas Phase Wittig Reaction of Non-Stabilized, Semi-Stabilized and Stabilized Me_3P and Ph_3P Phosphorus Ylides with Monocyclic Ketone: A Computational Study. *Comput. Theor. Chem.* **2016**, *1093*, 29−39. (d) Firaha, D. S.; Gibalova, A. V.; Holloczki, O. Basic Phosphonium Ionic Liquids as Wittig Reagents. *ACS Omega* **2017**, *2*, 2901−2911. (e) Adda, A.; Hadjadj-Aoul, R.; Lebsir, F.; Krallafa, A. M. Ab initio Static and Metadynamics Investigations of the Wittig Reaction. *Theor. Chem. Acc.* **2018**, *137*, 94. (f) Farfán, P.; Gómez, S.; Restrepo, A. On the Origins of Stereoselectivity in the Wittig Reaction. *Chem. Phys. Lett.* **2019**, *728*, 153−155. (g) Farfán, P.; Gómez, S.; Restrepo, A. Dissection of the Mechanism of the Wittig Reaction. *J. Org. Chem.* **2019**, *84*, 14644−14658.

(27) For recent calculations support this finding, see: (a) Kyri, A. W.; Gleim, F.; García Alcaraz, A.; Schnakenburg, G.; Espinosa Ferao, A.; Streubel, R. "Low-Coordinate" 1,2-Oxaphosphetanes − a new Opportunity in Coordination and Main Group Chemistry. *Chem. Commun.* **2018**, *54*, 7123−7126. (b) Espinosa Ferao, A. On the Mechanism of Trimethylphosphine-Mediated Reductive Dimerization of Ketones. *Inorg. Chem.* **2018**, *57*, 8058−8064. (c) Chamorro, E.; Duque-Noreña, M.; Gutiérrez-Sánchez, N.; Rincón, E.; Domingo, L. R. A Close Look to the Oxaphosphetane Formation along the Wittig Reaction: A [2 + 2] Cycloaddition? *J. Org. Chem.* **2020**, *85*, 6675−6686.

(28) Vedejs, E.; Marth, C. F. Oxaphosphetane Pseudorotation: Rates and Mechanistic Significance in the Wittig Reaction. *J. Am. Chem. Soc.* **1989**, *111*, 1519−1520.

(29) For assigning the absolute configuration of a pentacoordinated stereogenic center with a tbp geometry, see: Martin, J. C.; Balthazor, T. M. Sulfuranes. 22. Stereochemical Course of an Associative Displacement at Tetracoordinate Sulfur(IV) in a Sulfurane of Known Absolute Configuration. A Proposed System of Nomenclature for Optically Active Pentacoordinate Species. *J. Am. Chem. Soc.* **1977**, *99*, 152−162.

(30) Repeating three times the decomposition of **9a** at temperatures of 120, 130, 140, and 160 °C afforded *k* values with average deviations of 2, 1, 1, and 1%, respectively. Throughout this study, it was assumed that the maximum error of the *k* obtained does not exceed 2%.

(31) Further support to the appearance of a partial positive charge on carbon C4 during olefination was obtained by negative $\rho = -0.22$ ($r = 0.998$) obtained from a Hammett plot for the decomposition of **9c**,**f**,**g**,**h**

https://dx.doi.org/10.1021/acs.joc.0c01270
J. Org. Chem. XXXX, XXX, XXX−XXX

(Table 1, Figure S5). Hansch, C.; Leo, A.; Taft, R. W. A Survey of Hammett Substituent Constants and Resonance and Field Parameters. *Chem. Rev.* **1991**, *91*, 165−195.
(32) Berry, R. S. Correlation of Rates of Intramolecular Tunneling Processes, with Application to Some Group V Compounds. *J. Chem. Phys.* **1960**, *32*, 933−938.
(33) Couzijn, E. P. A.; Slootweg, J. C.; Ehlers, A. W.; Lammertsma, K. Stereomutation of Pentavalent Compounds: Validating the Berry Pseudorotation, Redressing Ugi's Turnstile Rotation, and Revealing the Two- and Three-Arm Turnstiles. *J. Am. Chem. Soc.* **2010**, *132*, 18127−18140.
(34) Alternatives exist for improving the accuracy of the results by more extensive consideration of dispersive forces in the calculations. (a) Zhao, Y.; Truhlar, D. G. The M06 Suite of Density Functionals for Main Group Thermochemistry, Thermochemical Kinetics, Noncovalent Interactions, Excited States, and Transition Elements: Two New Functionals and Systematic Testing of Four M06-Class Functionals and 12 Other Functionals. *Theor. Chem. Acc.* **2008**, *120*, 215−241. (b) Grimme, S. Density Functional Theory with London Dispersion Corrections. *Wiley Interdiscip. Rev.: Comput. Mol. Sci.* **2011**, *1*, 211−228.
(35) Frisch, M. J.; Trucks, G. W.; Schlegel, H. B.; Scuseria, G. E.; Robb, M. A.; Cheeseman, J. R.; Scalmani, G.; Barone, V.; Mennucci, B.; Petersson, G. A.; Nakatsuji, H.; Caricato, M.; Li, X.; Hratchian, H. P.; Izmaylov, A. F.; Bloino, J.; Zheng, G.; Sonnenberg, J. L.; Hada, M.; Ehara, M.; Toyota, K.; Fukuda, R.; Hasegawa, J.; Ishida, M.; Nakajima, T.; Honda, Y.; Kitao, O.; Nakai, H.; Vreven, T.; Montgomery, J. A., Jr.; Peralta, J. E.; Ogliaro, F.; Bearpark, M.; Heyd, J. J.; Brothers, E.; Kudin, K. N.; Staroverov, V. N.; Kobayashi, R.; Normand, J.; Raghavachari, K.; Rendell, A.; Burant, J. C.; Iyengar, S. S.; Tomasi, J.; Cossi, M.; Rega, N.; Millam, M. J.; Klene, M.; Knox, J. E.; Cross, J. B.; Bakken, V.; Adamo, C.; Jaramillo, J.; Gomperts, R.; Stratmann, R. E.; Yazyev, O.; Austin, A. J.; Cammi, R.; Pomelli, C.; Ochterski, J. W.; Martin, R. L.; Morokuma, K.; Zakrzewski, V. G.; Voth, G. A.; Salvador, P.; Dannenberg, J. J.; Dapprich, S.; Daniels, A. D.; Farkas, Ö.; Foresman, J. B.; Ortiz, J. V.; Cioslowski, J.; Fox, D. J. *Gaussian 09*, Revision B.01; Gaussian, Inc.: Wallingford, CT, 2010.
(36) Jastrzebski, J. T. H.; Boersma, J.; Esch, P. M.; van Koten, G. Intramolecular Penta- and Hexacoordlnate Tetraorganotin Compounds Containing the 8-(Dimethylamino)-1-naphthyl Ligand. *Organometallics* **1991**, *10*, 930−935.
(37) (a) Mari, F.; Lahti, P. M.; McEwen, W. E. Molecular Modeling of Oxaphosphetane Intermediates of Wittig Olefination Reactions. *Heteroat. Chem.* **1990**, *1*, 255−259. (b) Yamataka, H.; Nagase, S. Theoretical Calculations on the Wittig Reaction Revisited. *J. Am. Chem. Soc.* **1998**, *120*, 7530−7536.
(38) Restrepo-Cossio, A. A.; Gonzalez, C. A.; Mari, F. Comparative ab Initio Treatment (Hartree−Fock, Density Functional Theory, MP2, and Quadratic Configuration Interactions) of the Cycloaddition of Phosphorus Ylides with Formaldehyde in the Gas Phase. *J. Phys. Chem. A* **1998**, *102*, 6993−7000.
(39) (a) Alagona, G.; Ghio, C. Stepwise versus Concerted Mechanisms in the Wittig Reaction in Vacuo and in THF: The Case of 2,4-Dimethyl-3-pyrrol-1-yl-pentanal and Triphenylphosphonium Ylide. *Theor. Chem. Acc.* **2009**, *123*, 337−346. (b) Alagona, G.; Ghio, C. Free Energy Landscapes in THF for the Wittig Reaction of Acetaldehyde and Triphenylphosphonium Ylide. *Int. J. Quantum Chem.* **2010**, *110*, 2509−2521.
(40) Marenich, A. V.; Cramer, C. J.; Truhlar, D. G. Universal Solvation Model Based on Solute Electron Density and on a Continuum Model of the Solvent Defined by the Bulk Dielectric Constant and Atomic Surface Tensions. *J. Phys. Chem. B* **2009**, *113*, 6378−6396.
(41) (a) Vollbrecht, S.; Vollbrecht, A.; Jeske, J.; Jones, P. G.; Schmutzler, R.; du Mont, W.-W. Unusual Ring-Closure Reactions During the Oxidation of 1,1′-Bi(3-methyl- phosphol-2-ene) with Hexafluoroacetone - Formation of a Tricyclic Fluorine-Containing Phosphorane. *Chem. Ber.* **1997**, *130*, 819−822. (b) Kobayashi, J.; Kawashima, T. Chemistry of Pentacoordinated Anti-Apicophilic Phosphorus Compounds. *C. R. Chim.* **2010**, *13*, 1249−1259.
(42) (a) Barluenga, J.; Ferrero, M.; López, F.; Palacios, F. Reaction of α-Metallated *N*-Acyl-λ^5-phosphazenes with Aryl Cyanides. *J. Chem. Soc., Perkin Trans. 1* **1989**, 615−618. (b) Barluenga, J.; López, F.; Palacios, F. Reactions of *N*-Alkoxycarbonyl Alkyldiphenyl-λ^5-phosphazenes with Acetylene Esters. Synthesis of 1-Aza-2-oxo-4λ^5-phosphinines. *J. Organomet. Chem.* **1990**, *382*, 61−67.
(43) Álvarez-Gutiérrez, J. M.; Peralta-Pérez, E.; Pérez-Álvarez, I.; López-Ortiz, F. Reactions of Lithiated P-Diphenyl(alkyl)(*N*-methoxycarbonyl)phosphazenes with Michael Acceptors and Aldehydes. Synthesis of 1*H*-1,2-Azaphosphinin-6-ones, β-Hydroxy(*N*-methoxycarbonyl)phos-phazenes and 5,6-Dihydro-1,3,4-oxazaphosphinin-2-ones. *Tetrahedron* **2001**, *57*, 3075−3086.
(44) Bernard, M.; St. Jacques, M. Etude par Résonance Magnétique Nucléaire à Température Variable de Composés Apparentés au Méthylènecyclohexane. *Can. J. Chem.* **1970**, *48*, 3039−3044.
(45) Van der Linde, R.; Korver, O.; Korver, P. K.; van der Haak, P. J.; Veenland, J. U.; de Boer, Th. J. Proton Magnetic Resonance Spectra of Some 1,1-Diarylalkenes. *Spectrochim. Acta* **1965**, *21*, 1893−1898.
(46) Satoh, M.; Miyaura, N.; Suzuki, A. Stereo- and Regiospecific Synthesis of Trisubstituted Alkenes via the Palladium-catalyzed Cross-coupling Reaction of Diisopropyl (*E*)-(1-Alkyl-1-alkenyl)boronates with Organic Halides. *Chem. Lett.* **1986**, *15*, 1329−1332.
(47) Glattfeld, J. W. E.; Milligan, C. H. The Preparation of Optically Active Hydrazines. I. The Preparation of DL-*p*-Trimethylethylphenylhydrazine. The Isolation of Pure D-*p*-Trimethylethyl-aniline. *J. Am. Chem. Soc.* **1920**, *42*, 2322−2328.
(48) Boudier, A.; Darcel, C.; Flachsmann, F.; Micouin, L.; Oestreich, M.; Knochel, P. Stereoselective Preparation and Reactions of Configurationally Defined Dialkylzinc Compounds. *Chem. - Eur. J.* **2000**, *6*, 2748−2761.
(49) Rappoport, Z.; Gal, A. Vinylic Cations from Solvolysis. Part XIII. S_N1 and Electrophilic Addition−Elimination Routes in the Solvolysis of α-Bromo- and α-Chloro-4-methoxystyrenes. *J. Chem. Soc., Perkin Trans. 2* **1973**, 301−310.
(50) Bosch, H. W.; Hung, H. U.; Nietlispach, D.; Salzer, A. General Route to the Half-Open Ruthenium Metallocenes C_5Me_5Ru(pentadienyl) and C_5Me_5Ru(diene)Cl. X-ray Structures of an Optically Active Half-Open Metallocene and of a Dimetallic Ruthenabenzene Complex. *Organometallics* **1992**, *11*, 2087−2098.
(51) Danheiser, R. L.; Nowick, J. S. A Practical and Efficient Method for the Synthesis of.beta.-Lactones. *J. Org. Chem.* **1991**, *56*, 1176−1185.
(52) Wolf, J.; Brandt, L.; Fries, A.; Werner, H. Rhodium-Catalyzed Synthesis of Trisubstituted Olefins from Ethene Derivatives and Diazoalkanes. *Angew. Chem., Int. Ed. Engl.* **1990**, *29*, 510−512.
(53) Hooft, R. W. W. *COLLECT*; Nonius BV: Delft, The Netherlands, 1998.
(54) Otwinowski, Z.; Minor, W. Processing of X-ray Diffraction Data Collected in Oscillation Mode. *Methods Enzymol.* **1997**, *276*, 307−326.
(55) Area-Detector Software Package. *SMART & SAINT*; Bruker, 2007.
(56) Oxford Diffraction. *CrysAlis CCD and CrysAlis RED*; Oxford Diffraction Ltd: Abingdon, England, 2006.
(57) Altomare, A.; Cascarano, G.; Giacovazzo, C.; Guagliardi, A.; Burla, M. C.; Polidori, G.; Camalli, M. SIR92 - a Program for Automatic Solution of Crystal Structures by Direct Methods. *J. Appl. Crystallogr.* **1994**, *27*, 435.
(58) Burla, M. C.; Caliandro, R.; Camalli, M.; Carrozzini, B.; Cascarano, G. L.; De Caro, L.; Giacovazzo, C.; Polidori, G.; Spagna, R. SIR2004: an Improved Tool for Crystal Structure Determination and Refinement. *J. Appl. Crystallogr.* **2005**, *38*, 381−388.
(59) Beurskens, P. T.; Beurskens, G.; de Gelder, R.; García-Granda, S.; Gould, R. O.; Smits, J. M. M. *The DIRDIF-99 Program System*; Technical Report of the Crystallography Laboratory, University of Nijmegen: The Netherlands, 2008.
(60) Parkin, S.; Moezzi, B.; Hope, H. XABS2: an Empirical Absorption Correction Program. *J. Appl. Crystallogr.* **1995**, *28*, 53−56.
(61) Sheldrick, G. M. A Short History of SHELX. *Acta Crystallogr., Sect. A: Found. Crystallogr.* **2008**, *64*, 112−122.

https://dx.doi.org/10.1021/acs.joc.0c01270
J. Org. Chem. XXXX, XXX, XXX−XXX

(62) Farrugia, L. J. WinGX Suite for Small-Molecule Single-Crystal Crystallography. *J. Appl. Crystallogr.* **1999**, *32*, 837−838.
(63) Allen, F. H.; Johnson, O.; Shields, G. P.; Smith, B. R.; Towler, M. CIF Applications. XV. enCIFer: a Program for Viewing, Editing and Visualizing CIFs. *J. Appl. Crystallogr.* **2004**, *37*, 335−338.
(64) (a) Spek, A. L. PLATON, An Integrated Tool for the Analysis of the Results of a Single Crystal Structure Determination. *Acta Crystallogr. A* **1990**, *46*, C34. (b) Spek, A. L. PLATON, *A Multipurpose Crystallographic Tool*; Utrecht University: Utrecht, The Netherlands, 1998.
(65) Farrugia, L. J. ORTEP-3 for Windows - a Version of ORTEP-III with a Graphical User Interface (GUI). *J. Appl. Crystallogr.* **1997**, *30*, 565.
(66) Glendening, E. D.; Reed, A. E.; Carpenter, J. E.; Weinhold, F. *NBO*, Version 3.1.
(67) (a) Rassolov, V. A.; Ratner, M. A.; Pople, J. A.; Redfern, P. C.; Curtiss, L. A. 6-31G* Basis Set for Third-Row Atoms. *J. Comput. Chem.* **2001**, *22*, 976−984. (b) Zhao, Y.; Truhlar, D. G. A New Local Density Functional for Main-Group Thermochemistry, Transition Metal Bonding, Thermochemical Kinetics, and Noncovalent Interactions. *J. Chem. Phys.* **2006**, *125*, 194101.
(68) (a) González, C.; Schlegel, H. B. An Improved Algorithm for Reaction Path Following. *J. Chem. Phys.* **1989**, *90*, 2154−2161. (b) González, C.; Schlegel, H. B. Reaction Path Following in Mass-Weighted Internal Coordinates. *J. Phys. Chem.* **1990**, *94*, 5523−5527.
(69) The *trans*/*cis* descriptors indicate the relative orientation of the methyl group and *P*-phenyl groups.

https://dx.doi.org/10.1021/acs.joc.0c01270
J. Org. Chem. XXXX, XXX, XXX−XXX